Mixed Elements for the Analysis of Anisotropic Multilayered Piezoelectric Plates

E. CARRERA,[1,*] A. BÜTTNER[2] AND P. NALI[1]

[1]*Department of Aeronautics and Space Engineering, Politecnico di Torino, Torino, Italy*

[2]*Institut für Statik und Dynamik der Luft- und Raumfahrtkonstruktionen, University of Stuttgart, Germany*

ABSTRACT: Mixed plate elements for accurate evaluation of transverse mechanical stresses and electrical displacement are developed and compared in this work. Various forms of the Reissner mixed variational theorem are considered to *a priori* fulfill the interlaminar continuity of transverse electromechanical variables. Classical formulation based on the principle of virtual displacements are implemented for comparison purposes. 2D assumptions are introduced by means of the Carrera unified formulation (CUF). Layer-wise theories are developed by using Legendre type polynomials of various order in the plate-thickness expansion. The evaluation of the interlaminar continuity of transverse electric displacement and/or transverse stresses on the static response of piezoelectric actuated/sensing plate is provided and compared. Orthotropic and anisotropic simply supported plates are considered. Results are assessed by comparison with available 3D piezoelasticity solutions. The mixed formulations that *a priori* evaluate the transverse electric displacement appear of particular interest. These last, in fact, permit an easy, convenient and reliable calculation of the electric charge and make feasible the development of robust control algorithms.

Key Words: finite elements, multilayered plates, electro-mechanical problems, classical and mixed formulations, smart structures.

INTRODUCTION

Background

SMART systems are the candidate for next generation structures of aerospace vehicles as well as for some advanced products of automotive and ship industries. Many research activities are known to design a ''smart wing system'' able to introduce strong benefits in the green area. Piezoelectric materials are extensively used in that framework. These materials are characterized by the so called ''direct'' and ''inverse effect'': an applied mechanical stresses induces electrical potential and vice versa. Such an electro-mechanical coupling permits one to build up closed-loop control systems in which piezo-materials play the role of both actuators and sensors. An intelligent structure can be therefore built in which, for instance, deformations or vibrations are reduced by appropriate control laws.

A number of theoretical and practical problems arise in the applications, whose solution would play a crucial role in the future development of smart structures. The following are herein mentioned: the low saturation value of the electric voltage can lead to severe limitation for the magnitude of the forces that can be generated by a given actuator; the difficulties in developing efficient technology for the integration of piezoelectric materials in both continuous and distributed forms; the result of design of an effective, efficient, and robust real time control could not always be possible. The realization of an efficient and intelligent network, fully integrated in the structures, which makes the use of embedded piezoelectric materials convenient with respect to other traditional sensors and actuators must be completely demonstrated. An exhaustive discussion on the above, can be read in the two articles by Chopra (1996, 2002) and related literature.

2D Modeling

However, an appropriate use of piezoelectric materials, requires an accurate description of electrical and mechanical fields in the constitutive layers. Pionering works on piezoelasticity are those by Mindlin (1952), Tiersten and Mindlin (1962), Eer Nisse (1967a) as well as the book by Tiersten (1969). This article focuses on the computational, finite elements (FEs),

*Author to whom correspondence should be addressed.
E-mail: pietro.nali@polito.it
Figures 1–6 appear in color online: http://jim.sagepub.com

1045-389X/10/07 0701–17 $10.00/0 DOI: 10.1177/1045389X10364864

electro-mechanical 2D modelings of smart structures embedding piezoelectric layers.

Piezoelectric plates appear as multilayered structures. Piezoelectric layers are often embedded in laminated structures made by anisotropic composite materials. Accurate modeling of these structures requires appropriate description of mechanical and electrical variables in the thickness plate direction. Zig-zag (ZZ) form of displacement fields, interlaminar continuity (IC) of transverse shear and normal stress components (Carrera, 2003a) and electrical displacements must be mandatorily accounted for in a reliable analysis. In the work of Carrera (1995), ZZ and IC were referred to as C_z^0-Requirements (see Section 4.1). The importance of appropriate modelings of piezoelectric plates is clearly displayed by the large amount of papers that have been published in the last two decades. Available FEs have been developed accounting to various plate theories:

(1) Classical plate analysis: classical lamination theory (CLT) and first order shear deformation theory (FSDT);
(2) Refinements of classical theories (higher order theory, HOT);
(3) Zig-zag theories (Lekhnitskii, 1935; Ambartusumian, 1958; Reissner, 1984; Carrera, 2003a);
(4) Layer-wise (LW) theories, in which the variables are defined in each layer (while the same variables are used for the whole multilayered structure in the so-called equivalent single-layer (ESL) models);
(5) Formulation with displacement or stress unknowns and mixed ones.

A first FE formulation based on the early works of Mindlin (1952) and Eer Nisse (1967b) have been proposed by Allik and Hughes (1970). Among the available review papers, those by Saravanos and Heyliger (1999), Benjeddou (2000), and Wang and Yang (2000) are herein mentioned. A short review of some of the latest contribution to FE analysis of piezoelectric plates follows. Application of piezoelectric shell elements to vibration control was provided by Lammering (1991). LW plate elements with mechanical displacements and electric voltage as field variables were proposed by Heyliger, Ramirez and Saravanos (1994a); application were given to static problems with applied surface tractions and specified surface potentials. The extension to the dynamic case was presented by Saravanos et al. (1997). An FE accounting for a FSDT description of displacement and LW form of the electric potential has more recently been developed by Sheik et al. (2001). The numerical, membrane and bending behavior of FEs which are based on FSDT has been analyzed by Auricchio et al. (2001) in the framework of a suitable variational formulation. A modeling technique for piezolaminated plates using layerwise mixed FEs has been proposed by Garcia Lage et al. (2004a, b). Third order theory of HOT type has been applied by Thornburg and Chattopadhyay (2002) to derive FEs accounting for electro-mechanical coupling. Similar elements have been more recently considered by Shu (2005). An extension of third order ZZ Ambartsumian multilayered theory to finite analysis of electromechanical problems has been proposed by Oh and Cho (2004). Another extension to piezoelectric numerically efficient plate/shell elements based on mixed interpolation of tensorial components (MITC) formulation has been recently provided by Kögl and Buchalem (2005a, b).

The Contribution of the Reissner Mixed Variational Theorem

Since almost one decade, Carrera et al. (1995, 1996, 2001) have contributed to the application of Reissner mixed variational theorem (RMVT) to multilayered made structures. Closed form solution analyses (Carrera, 1998, 2000) as well as FE applications (Carrera and Demasi, 2002a, b) have shown that RMVT consists of a very suitable tool to provide quasi-3D description of stress and strain fields in anisotropic laminated structures. RMVT was employed in the framework of the Carrera unified formulation (CUF) (Carrera, 2003b). In particular, the CUF permits one to formulate both ESL and LW models in terms of a few fundamental nuclei whose form does not depends on neither the order of expansion (that have been used for the various variables) nor by the number of the node of element.

A first application of RMVT to piezoelectric plates was provided by Carrera (1997): an MITC type plate element was extended to non-linear dynamic analysis of piezoelectric composite plate. The CUF has been applied, in the principle of virtual displacements (PVD) framework, to piezoelectric plate. The attention was restricted to analytical closed form solutions (Ballhause, 2004). Extension of related FEs to the free vibration problems was given by Robaldo et al. (2006). RMVT closed form solutions were presented by D'Ottavio and Kröplin (2006), while extension to shell was provided by Carrera and Brischetto (2005). Attempts to extend RMVT to piezoelectric plates were also made by Benjeddou and Andrianarison (2005); numerical results were not provided in the last paper. A substantiation of the RMVT extension to piezoelectric continuous can be reffered to in D'Ottavio and Kröplin (2006). RMVT has also been applied by Garcia Lage et al. (2004) to develop LW plate elements in the static case. Transverse component of electric displacement was also considered as an assumed variable. Attention was restricted to quadratic distribution of displacements (mechanical and electrical) and transverse stress unknowns in the static cases. Recent FE applications of RMVT to piezoelectric plates have been provided by Carrera et al. (2007, 2008a, 2009). The first work

includes the electrical stiffness in the RMVT with only transverse stress variables modeled. In 2008, the electrical transverse displacement was modeled via RMVT together with transverse stresses. In 2009, RMVT was applied only to the electrical transverse displacement. Results were in the above work restricted to orthotropic plates analysis.

Many previous authors' findings are devoted to RMVT and a number of new FEs where derived and systematically compared to classical ones which were formulated on the basis of PVD applications. ESL and LW variable descriptions analysis where compared to 3D available solutions. Upto fourth order expansions along the through-the-thickness plate/layers direction was considered for the problem variables.

With respect to previous papers, the present one proposes the calculation of the FE fundamental nuclei according to a recently formulated condensed notation (Carrera et al. 2009), leading to a more efficient calculation of the FE stiffness matrix. Moreover, FEs derived form two mixed variational statements are herein compared: the RMVT-D_z-σ_n, by which the evaluation of the IC of transverse electric displacement and transverse stresses is provided, and the RMVT-D_z, where only the IC of transverse electric displacement is accounted for. The latter variational statement involves a lower number of degrees of freedom (DOF) in the analysis, leads to accurate results for the transverse electric displacement, while it cannot provide the same accuracy of RMVT-D_z-σ_n for the evaluation of transverse stresses. A few results related to to anisotropic piezoelectric plates are also included.

The article has been organized as the following. The next section 2 quotes the referred variational statements, e.g., PVD and RMVT form suitable for piezoelectric continua. The variationally consistent constitutive equations are derived in the section 'Constitutive Relations'. CUF is described in the section 'Through-the-thickness Assumptions of Primary Variables via Carrera Unified Formulation'. Fundamental nuclei related to the various matrices are derived in the section 'Fundamental Nuclei and Finite element Matrices'. Numerical results are discussed in the section 'Numerical Results and Discussion' to which concluding remarks follow. Explicit form of the RMVT-D_z-σ_n fundamental nucleus, is quoted in the Appendix.

CONSIDERED VARIATIONAL STATEMENTS

The Principle of Virtual Displacements for the Electro-mechanical Case

The PVD statement for the pure-mechanical case study is commonly written as follows:

$$\int_V \left(\delta\boldsymbol{\epsilon}_G^T \boldsymbol{\sigma}_H\right) \mathrm{d}V = \delta L_e, \tag{1}$$

where superscript "T" indicates the array transposition, δ is the variational symbol and bold letters denote arrays. Subscripts "G" and "H" indicate variables obtained by geometrical relations and by constitutive/Hooke's relations, respectively. σ, ϵ and L_e indicate stresses, strains and the external work, respectively.

In the case of applied electro-mechanical loading on a surface Ω, employing Einstein's summation convention over repeated indices, the virtual variation of the external work can be expressed as:

$$\delta L_e = \int_\Omega \left(\bar{t}_i\, \delta u_i - \bar{Q}\, \delta\phi\right) \mathrm{d}\Omega, \tag{2}$$

where $\bar{t}_i$ is the mechanical loading in i-direction (pressure), u_i is the displacement component in i-direction, $\bar{Q}$ is the charge density on the plate surface, ϕ is the electric potential.

Stresses and strains are conveniently split between in-plane and out-of-plane (normal or transverse) components (Carrera et al. 2009):

$$\int_V (\delta\boldsymbol{\epsilon}_{pG}^T \boldsymbol{\sigma}_{pH} + \delta\boldsymbol{\epsilon}_{nG}^T \boldsymbol{\sigma}_{nH})\, \mathrm{d}V = \delta L_e, \tag{3}$$

with

$$\boldsymbol{\epsilon}_p^T = \left\{ \epsilon_{xx} \quad \epsilon_{yy} \quad \epsilon_{xy} \right\}; \quad \boldsymbol{\sigma}_p^T = \left\{ \sigma_{xx} \quad \sigma_{yy} \quad \sigma_{xy} \right\};$$
$$\boldsymbol{\epsilon}_n^T = \left\{ \epsilon_{zz} \quad \epsilon_{xz} \quad \epsilon_{yz} \right\}; \quad \boldsymbol{\sigma}_n^T = \left\{ \sigma_{zz} \quad \sigma_{xz} \quad \sigma_{yz} \right\}.$$

Cartesian x, y, z reference system is considered and the notations are already used in previous works (Carrera and Fagiano, 2008). Subscript "p" denotes in-plane unknowns and subscript "n" denotes out-of-plane unknowns; subscript "z" indicates the through-the-thickness z-direction, while subscripts "x" and "y" are for the two in-plane directions.

If electrical contributions are included, the PVD in Equation (3) becomes:

$$\int_V \left(\delta\boldsymbol{\epsilon}_{pG}^T \boldsymbol{\sigma}_{pH} + \delta\boldsymbol{\epsilon}_{nG}^T \boldsymbol{\sigma}_{nH}\delta - \delta\boldsymbol{E}_{pG}^T \boldsymbol{D}_{pH} - \delta E_{nG} D_{nH}\right) \mathrm{d}V = \delta L_e, \tag{4}$$

with:

$$\boldsymbol{E}_p^T = \left\{ E_x \quad E_y \right\}; \quad \boldsymbol{D}_p^T = \left\{ D_x \quad D_y \right\};$$
$$E_n = \{\, E_z \,\}; \quad D_n = \{D_z\}.$$

D and E indicate the electric displacement and the electric field, respectively.

The condensed vectorial notation introduced by Carrera et al. (2009) is employed in this work. The two multifield variables are introduced:

$$\boldsymbol{\mathcal{S}}^T = \left\{ \sigma_{xx} \quad \sigma_{yy} \quad \sigma_{xy} \quad -D_x \quad -D_y \quad \sigma_{zz} \quad \sigma_{xz} \quad \sigma_{yz} \quad -D_z \right\}, \tag{5}$$

$$\boldsymbol{\mathcal{E}}^T = \left\{ \epsilon_{xx} \quad \epsilon_{yy} \quad \epsilon_{xy} \quad E_x \quad E_y \quad \epsilon_{zz} \quad \epsilon_{xz} \quad \epsilon_{yz} \quad E_z \right\}, \tag{6}$$

where $\boldsymbol{\mathcal{S}}$ is the vector of extensive variables and $\boldsymbol{\mathcal{E}}$ is the vector of intensive ones. D_z and D_n are the same quantity expressed in different notations.

It is possible to rewrite Equation (4) in form as simple as Equation (1) for multifield problems:

$$\int_V \left(\delta \boldsymbol{\mathcal{E}}_G^T \boldsymbol{\mathcal{S}}_H\right) \mathrm{d}V = \delta L_e. \tag{7}$$

For multilayered structures, the volume integral, has to be intended as:

$$\int_V (\ldots)\,\mathrm{d}V = \sum_{k=1}^{N_l} \int_{\Omega_k} \int_{A_k} (\ldots)\,\mathrm{d}\Omega_k\,\mathrm{d}z, \tag{8}$$

where Ω_k is the layer middle surface; A_k denotes the layer-thickness domain and N_l indicates the number of layers.

The RMVT-D_z-$\boldsymbol{\sigma}_n$

The advantage of using RMVT consists in the possibility of assuming two independent set of variables: a set of primary unknowns and a set of extensive variables which are modeled in the thickness plate in the z-direction. This leads to the *a priori* and complete fulfillment of the IC for the modeled extensive variables, with consequent satisfaction of the C_z^0 requirements in Carrera (1996). The RMVT has been commonly employed to obtain accurate results for transverse stresses in pure mechanical problems (Reissner, 1984). In piezoelectric applications, RMVT has been recently extended to model the transverse electric displacement other than normal stresses (Carrera and Boscolo, 2007).

The RMVT statement with *a priori* modeling of the transverse electric displacement D_z (or D_n) and transverse stresses $\boldsymbol{\sigma}_n$ is here called RMVT-D_z-σ_n and it appears in literature according to the following form (Carrera et al. 2009):

$$\int_V \Big(\delta \boldsymbol{\epsilon}_{pG}^T \boldsymbol{\sigma}_{pH} + \delta \boldsymbol{\epsilon}_{nG}^T \boldsymbol{\sigma}_{nH} - \delta \boldsymbol{E}_{pG}^T \boldsymbol{D}_{pH} - \delta E_{nG} D_n + \delta \boldsymbol{\sigma}_{nM}^T (\epsilon_{nG} - \epsilon_{nH}) - \delta D_n (E_{nG} - E_{nH})\Big) \mathrm{d}V = \delta L_e. \tag{9}$$

By referring to the condensed notation and considering that subscript "a" indicates " not modeled quantities", while subscript "b" is related to "modeled quantities", the following vectors can be introduced:

$\boldsymbol{\mathcal{S}}_{aH} = \{\ \sigma_{xx}\ \sigma_{yy}\ \sigma_{xy}\ -D_x\ -D_y\ \}_H$ is the vector of not-modeled extensive variables, which are calculated by constitutive relations;

$\boldsymbol{\mathcal{S}}_b = \{\ \sigma_{zz}\ \sigma_{xz}\ \sigma_{yz}\ -D_z\ \}$ is the vector of modeled extensive variables;

$\boldsymbol{\mathcal{E}}_{aG} = \{\ \epsilon_{xx}\ \epsilon_{yy}\ \epsilon_{xy}\ E_x\ E_y\ \}_G$ is the vector of intensive variables associated to $\boldsymbol{\mathcal{S}}_a$ and calculated by geometrical relations;

$\boldsymbol{\mathcal{E}}_{bG} = \{\ \epsilon_{zz}\ \epsilon_{xz}\ \epsilon_{yz}\ E_z\ \}_G$ is the vector of intensive variables associated to $\boldsymbol{\mathcal{S}}_b$ and calculated by geometrical relations;

$\boldsymbol{\mathcal{E}}_{bH} = \{\ \epsilon_{zz}\ \epsilon_{xz}\ \epsilon_{yz}\ E_z\ \}_H$ is the vector of intensive variables associated to $\boldsymbol{\mathcal{S}}_b$ and calculated by constitutive relations.

In doing so, the RMVT statement with *a priori* modeling of the transverse electric displacement D_z and transverse stresses $\boldsymbol{\sigma}_n$ takes the following form:

$$\int_V \left(\delta \boldsymbol{\mathcal{E}}_{aG}^T \boldsymbol{\mathcal{S}}_{aH} + \delta \boldsymbol{\mathcal{E}}_{bG}^T \boldsymbol{\mathcal{S}}_b + \delta \boldsymbol{\mathcal{S}}_b^T \left(\boldsymbol{\mathcal{E}}_{bG} - \boldsymbol{\mathcal{E}}_{bH}\right)\right) \mathrm{d}V = \delta L_e. \tag{10}$$

In the next section, the constitutive relations are obtained for the RMVT-D_z-$\boldsymbol{\sigma}_n$ variational statement in the condensed notation, according to Equation (10).

CONSTITUTIVE RELATIONS

Physical constitutive equations, which are suitable for the applications of the PVD, for the electro-mechanical case reduces to:

$$\begin{aligned} \sigma_{ij} &= C_{ij\,lm}\epsilon_{lm} - e_{ij\,l}E_l, \\ D_l &= e_{lij}\epsilon_{ij} + \varepsilon_{lm}E_m, \end{aligned} \tag{11}$$

where standard tensor notation is used and Einstein's summation convention is implied over repeated indices and with: $C_{ij\,lm}$ = elastic coefficients – Hooke's law; e_{lij} = piezoelectric coefficients; ϵ_{ij} = permittivity coefficients. Note that $2\epsilon_{ij}$ components in tensorial notation correspond to ϵ_{ij} components in vectorial notation, when $(i \neq j)$.

If the RMVT is considered, applying the variational statement of Equation (10), constitutive relations are obtained as it follows, according to the condensed notation.

For sake of clarity, it is convenient to specify that primary unknown variables are collected in the vector

$$\boldsymbol{V}^{kT} = \left\{ u_x^k \quad u_y^k \quad u_z^k \quad \phi^k \quad \sigma_{zz}^k \quad \sigma_{xz}^k \quad \sigma_{yz}^k \quad D_z^k \right\}$$

where the superscript k stands for the k-th layer. It is useful to rewrite vectors introduced in the previous section:

$$\begin{aligned} \boldsymbol{\mathcal{E}}_a^{kT} &= \left\{ \epsilon_{xx}^k \quad \epsilon_{yy}^k \quad \epsilon_{xy}^k \quad E_x^k \quad E_y^k \right\}; \\ \boldsymbol{\mathcal{E}}_b^{kT} &= \left\{ \epsilon_{zz}^k \quad \epsilon_{xz}^k \quad \epsilon_{yz}^k \quad E_z^k \right\}; \\ \boldsymbol{\mathcal{S}}_a^{kT} &= \left\{ \sigma_{xx}^k \quad \sigma_{yy}^k \quad \sigma_{xy}^k \quad -D_x^k \quad -D_y^k \right\}; \\ \boldsymbol{\mathcal{S}}_b^{kT} &= \left\{ \sigma_{zz}^k \quad \sigma_{xz}^k \quad \sigma_{yz}^k \quad -D_z^k \right\}. \end{aligned}$$

Following geometrical relations can be written:

$$\boldsymbol{\mathcal{E}}^k_{aG} = \boldsymbol{D}_a \boldsymbol{V}^k; \tag{12}$$

$$\boldsymbol{\mathcal{E}}^k_{bG} = \boldsymbol{D}_b \boldsymbol{V}^k; \tag{13}$$

$$\boldsymbol{\mathcal{S}}^k_{bG} = \boldsymbol{D}_{b'} \boldsymbol{V}^k, \tag{14}$$

where the differential matrices in explicit form read:

$$\boldsymbol{D}_a = \begin{pmatrix} \partial_x & 0 & 0 & 0 & 0 & 0 & 0 & 0 \\ 0 & \partial_y & 0 & 0 & 0 & 0 & 0 & 0 \\ \partial_y & \partial_x & 0 & 0 & 0 & 0 & 0 & 0 \\ 0 & 0 & 0 & -\partial_x & 0 & 0 & 0 & 0 \\ 0 & 0 & 0 & -\partial_y & 0 & 0 & 0 & 0 \end{pmatrix};$$

$$\boldsymbol{D}_b = \begin{pmatrix} 0 & 0 & \partial_z & 0 & 0 & 0 & 0 & 0 \\ \partial_z & 0 & \partial_x & 0 & 0 & 0 & 0 & 0 \\ 0 & \partial_z & \partial_y & 0 & 0 & 0 & 0 & 0 \\ 0 & 0 & 0 & -\partial_z & 0 & 0 & 0 & 0 \end{pmatrix};$$

$$\boldsymbol{D}_{b'} = \begin{pmatrix} 0 & 0 & 0 & 0 & 1 & 0 & 0 & 0 \\ 0 & 0 & 0 & 0 & 0 & 1 & 0 & 0 \\ 0 & 0 & 0 & 0 & 0 & 0 & 1 & 0 \\ 0 & 0 & 0 & 0 & 0 & 0 & 0 & -1 \end{pmatrix}.$$

Referring to the condensed notation and specifying which quantities are obtained by Hooke's law or by geometrical relations, one gets:

$$\widetilde{\boldsymbol{\mathcal{S}}}^k_H = \widetilde{\boldsymbol{H}}^k \widetilde{\boldsymbol{\mathcal{E}}}^k_G. \tag{15}$$

$\widetilde{\boldsymbol{\mathcal{S}}}^k_H$ is composed by the vector of not modeled extensive variables $\boldsymbol{\mathcal{S}}^k_{aH}$ and the vector of intensive variables $\boldsymbol{\mathcal{E}}_{bH}$ (which is associated to $\boldsymbol{\mathcal{S}}^k_b$); $\widetilde{\boldsymbol{\mathcal{E}}}^k_G$ is composed by the vector of intensive variables $\boldsymbol{\mathcal{E}}^k_{aG}$ (which is associated to $\boldsymbol{\mathcal{S}}^k_a$) and the vector of modeled extensive variables $\boldsymbol{\mathcal{S}}^k_b$, that can be thought as a geometrical vector, by Equation (14): $\widetilde{\boldsymbol{\mathcal{S}}}^{kT}_H = \{\, \boldsymbol{\mathcal{S}}^{kT}_{aH} \quad \boldsymbol{\mathcal{E}}^{kT}_{bH} \,\}$; $\widetilde{\boldsymbol{\mathcal{E}}}^{kT}_G = \{\, \boldsymbol{\mathcal{E}}^{kT}_{aG} \quad \boldsymbol{\mathcal{S}}^{kT}_{bG} \,\}$.

The physical constitutive matrix $\boldsymbol{H}^k$ can be partitioned by dividing cells related to modeled and not modeled quantities:

$$\boldsymbol{H}^k = \begin{Bmatrix} \boldsymbol{H}^k_{aa} & \boldsymbol{H}^k_{ab} \\ \boldsymbol{H}^k_{ba} & \boldsymbol{H}^k_{bb} \end{Bmatrix}, \tag{16}$$

where $\boldsymbol{H}^k_{ab} = \boldsymbol{H}^{kT}_{ba}$.

In explicit form:

$$\boldsymbol{H}^k_{aa} = \begin{pmatrix} C^k_{11} & C^k_{12} & C^k_{16} & 0 & 0 \\ C^k_{12} & C^k_{22} & C^k_{26} & 0 & 0 \\ C^k_{16} & C^k_{26} & C^k_{66} & 0 & 0 \\ 0 & 0 & 0 & -\varepsilon^k_{11} & -\varepsilon^k_{12} \\ 0 & 0 & 0 & -\varepsilon^k_{12} & -\varepsilon^k_{22} \end{pmatrix};$$

$$\boldsymbol{H}^k_{ab} = \begin{pmatrix} C^k_{13} & 0 & 0 & -e^k_{31} \\ C^k_{23} & 0 & 0 & -e^k_{32} \\ C^k_{36} & 0 & 0 & -e^k_{36} \\ 0 & -e^k_{15} & -e^k_{14} & 0 \\ 0 & -e^k_{25} & -e^k_{24} & 0 \end{pmatrix};$$

$$\boldsymbol{H}^k_{ba} = \begin{pmatrix} C^k_{13} & C^k_{23} & C^k_{36} & 0 & 0 \\ 0 & 0 & 0 & -e^k_{15} & -e^k_{25} \\ 0 & 0 & 0 & -e^k_{14} & -e^k_{24} \\ -e^k_{31} & -e^k_{32} & -e^k_{36} & 0 & 0 \end{pmatrix};$$

$$\boldsymbol{H}^k_{bb} = \begin{pmatrix} C^k_{33} & 0 & 0 & -e^k_{33} \\ 0 & C^k_{55} & C^k_{45} & 0 \\ 0 & C^k_{45} & C^k_{44} & 0 \\ -e^k_{33} & 0 & 0 & -\varepsilon^k_{33} \end{pmatrix}.$$

Physical constitutive relations, can be arranged according to the above partitioning:

$$\boldsymbol{\mathcal{S}}^k_{aH} = \boldsymbol{H}^k_{aa} \boldsymbol{\mathcal{E}}^k_{aG} + \boldsymbol{H}^k_{ab} \boldsymbol{\mathcal{E}}^k_{bG}, \quad \boldsymbol{\mathcal{S}}^k_{bH} = \boldsymbol{H}^k_{ba} \boldsymbol{\mathcal{E}}^k_{aG} + \boldsymbol{H}^k_{bb} \boldsymbol{\mathcal{E}}^k_{bG}. \tag{17}$$

From Equations (17) one has:

$$\boldsymbol{\mathcal{S}}^k_{aH} = \widetilde{\boldsymbol{H}}^k_{aa} \boldsymbol{\mathcal{E}}^k_{aG} + \widetilde{\boldsymbol{H}}^k_{ab} \boldsymbol{\mathcal{S}}^k_{bG}, \quad \boldsymbol{\mathcal{E}}^k_{bH} = \widetilde{\boldsymbol{H}}^k_{ba} \boldsymbol{\mathcal{E}}^k_{aG} + \widetilde{\boldsymbol{H}}^k_{bb} \boldsymbol{\mathcal{S}}^k_{bG}, \tag{18}$$

with:

$$\widetilde{\boldsymbol{H}}^k_{aa} = \boldsymbol{H}^k_{aa} - \boldsymbol{H}^k_{ab} (\boldsymbol{H}^k_{bb})^{-1} \boldsymbol{H}^k_{ba}; \quad \widetilde{\boldsymbol{H}}^k_{ab} = \boldsymbol{H}^k_{ab} (\boldsymbol{H}^k_{bb})^{-1};$$
$$\widetilde{\boldsymbol{H}}^k_{ba} = -(\boldsymbol{H}^k_{bb})^{-1} \boldsymbol{H}^k_{ba}; \quad \widetilde{\boldsymbol{H}}^k_{bb} = (\boldsymbol{H}^k_{bb})^{-1}.$$

Matrix $\widetilde{\boldsymbol{H}}^k$ of Equation (15) is:

$$\widetilde{\boldsymbol{H}}^k = \begin{Bmatrix} \widetilde{\boldsymbol{H}}^k_{aa} & \widetilde{\boldsymbol{H}}^k_{ab} \\ \widetilde{\boldsymbol{H}}^k_{ba} & \widetilde{\boldsymbol{H}}^k_{bb} \end{Bmatrix}. \tag{19}$$

To be noticed that matrix $\widetilde{\boldsymbol{H}}^k$ represents the constitutive relations suitable for the RMVT-D_z-σ_n in the form of Equation (10). The explicit form of $\widetilde{\boldsymbol{H}}^k$ can be found in the Appendix.

The advantage of using the condensed notation is that the above shown procedure to calculate constitutive relations is also applicable when different/more extensive variables are modeled through the thickness plate in the z-direction. It represents a general and an automatic way to calculate the constitutive coefficients for many different cases of variational statements (Carrera et al. 2009).

THROUGH-THE-THICKNESS ASSUMPTIONS OF PRIMARY VARIABLES VIA CARRERA UNIFIED FORMULATION

As it is well known in the open literature (Reddy, 1987, 1999), any 2D plate modeling introduces an expansion for the unknown in terms of thickness functions (Equation (20)). In the framework of the CUF (Carrera, 2002c, 2003a), the expansion in Equation (20) is considered in a convenient framework that generates "Fundamental Nuclei" (Appendix) whose form is not affected by the polynomials used as a basis in Equation (20) assumptions.

$$\boldsymbol{V}^k(x,y,z) = F_\tau(z)\ \boldsymbol{V}^k_\tau(x,y) \qquad \tau = 0,1,\ldots,\ N. \quad (20)$$

The repeated indexes are summed over their ranges. The polynomials $F_\tau(z)$ constitute a set of independent functions. Such base is arbitrarily chosen: power of z, Lagrange polynomials or a combination of Legendre polynomials can be considered. The expansion can be made at the layer level (LW description) or at the multilayered plate level (ESL description). N denotes the order of the introduced expansion. In case of RMVT-D_z-σ_n application, variables concerning displacements, transverse stresses, electrical potential and transverse electric displacement are included in vector $\boldsymbol{V}^k$.

It is understood that, by the arbitrary choice of the thickness expansion, the same computational code can address not just one FE, but a complete family of them, with different descriptions for primary unknowns along the thickness of the structure. In doing so, the CUF reduces a 3D problem to a 2D problem. The order of the variable's expansion along the thickness of the plate is taken as a free parameter of the FE and, in the developed code, it can be changed ranging from 1 upto 4.

By appropriately choosing the thickness functions, both ESL and LW descriptions along the thickness of the plate are admissible. In an ESL model, a global assumption for the unknown is considered along the thickness of the plate (i.e., a Taylor expansion) while, in a LW model, the expansion is made for each layer separately and then IC conditions are enforced by the assembly procedure. The latter leads generally to more accurate results but the number of the nodal DOF increases with the number of the layers coming out to a greater computational cost.

In the implemented code, for a LW theory the thickness functions are defined by:

$$F_t = \frac{P_0 + P_1}{2}, \quad F_b = \frac{P_0 - P_1}{2}, \quad F_r = P_r - P_{r-2} \quad r = 2,\ldots,\ N, \quad (21)$$

where $P_i = P_i(\zeta_k)$ is the *Legendre* polynomial of i-th order defined in the domain $-1 \le \zeta_k \le 1$. The chosen thickness functions have the interesting properties:

$$\zeta_k = \begin{cases} 1: & F_t = 1, \quad F_b = 0, \quad F_r = 0 \\ -1: & F_t = 0, \quad F_b = 1, \quad F_r = 0 \end{cases}. \quad (22)$$

Using these definitions, the generalized assumptions for the primary unknowns of the k-th layer in Equation (20) can be stated as:

$$\boldsymbol{V}^k(x,y,z) = F_b(z)\boldsymbol{V}^k_b(x,y) + F_r(z)\boldsymbol{V}^k_r(x,y) + F_t(z)\boldsymbol{V}^k_t(x,y) = F_\tau\ \boldsymbol{V}^k_\tau, \quad \text{with } r = 2,\ldots,N. \quad (23)$$

The variables $\boldsymbol{V}_b$ and $\boldsymbol{V}_t$ are the actual primary unknowns at the bottom and the top surfaces of the layer and the inter-laminar continuity can be easily imposed:

$$\boldsymbol{V}^k_t = \boldsymbol{V}^{(k+1)}_b, \quad \text{with } k = 1,\ldots,N_l - 1. \quad (24)$$

Acronyms are used for the implemented plate elements. These are denoted by LM1, LM2, LM3, LM4 in which: L states that an LW description is employed and M indicates that mixed approach based on the RMVT is used; 1–4 denotes the order of the expansion introduced for the field variables in each layer. If acronyms EM1, EM2, EM3, EM4 are used, an ESL description is employed. LD1, LD2, LD3, LD4 and ED1, ED2, ED3, ED4 are the corresponding acronyms when classical approach based on the PVD is used (letter D).

"FUNDAMENTAL NUCLEI" AND FINITE ELEMENT MATRICES

This section is devoted to the RMVT-D_z-σ_n variational statement, while the application of the corresponding PVD can be found in the previous paper of Carrera et al. (2009). RMVT-D_z variational statement is described in detail in the work of Carrera and Nali (2009).

FE Discretization

In case of FEM implementation, unknowns can be expressed in terms of their nodal values, via the shape functions N_i:

$$\boldsymbol{V}^k_\tau(x,y) = N_i(x,y)\boldsymbol{R}^k_{\tau i} \qquad i = 1,2,\ldots,N_n, \quad (25)$$

while for the virtual variations:

$$\delta\boldsymbol{V}^k_s(x,y) = N_j(x,y)\delta\boldsymbol{R}^k_{sj} \qquad j = 1,2,\ldots,N_n, \quad (26)$$

where N_n denotes the number of nodes concerning the considered FE and $\boldsymbol{R}^k_{\tau i}$ is the vector containing the nodal unknowns:

$$\boldsymbol{R}^{kT}_{\tau i} = \left\{ R^k_{u_x\tau i} \quad R^k_{u_y\tau i} \quad R^k_{u_z\tau i} \quad R^k_{\phi\tau i} \quad R^k_{\sigma_{zz}\tau i} \quad R^k_{\sigma_{xz}\tau i} \quad R^k_{\sigma_{yz}\tau i} \quad R^k_{D_z\tau i} \right\}. \quad (27)$$

The final expression of the primary unknowns is:

$$\boldsymbol{V}^k(x, y, z) = F_\tau N_i \boldsymbol{R}^k_{\tau i}. \tag{28}$$

Derivation of Fundamental Nuclei and FE matrices

Upon substitution of Equations (12)–(14), (18), (25) and (26), the variational statement in Equation (10) leads to a set of equilibrium equations which can be formally put in the following compact form:

$$\delta \boldsymbol{R}^k_{sj}: \quad \boldsymbol{K}^{k\tau sij}\, \boldsymbol{R}^k_{\tau i} = \boldsymbol{P}^k_{sj}, \tag{29}$$

where $\boldsymbol{P}^k$ is the vector of nodal loads and the related boundary conditions are $\overline{\boldsymbol{R}}^k$.

The number of obtained equations coincides with the number of introduced variables: τ and s vary from 0 to N, i and j vary from 1 to N_n and k ranges from 1 to N_l.

Matrix $\boldsymbol{K}^{k\tau sij}$ is the fundamental nucleus. In this case it is a 8×8 array and, more in general, it provides the information to build the stiffness matrix (The explicit form of $\boldsymbol{K}^{k\tau sij}$ can be found in the Appendix).

Whatever is the considered variational statement, starting from the fundamental nucleus, for a given discretization, the stiffness matrix $\boldsymbol{K}$ can be calculated by numerical integration and the assembly procedure. $\boldsymbol{K}$ is representative of the Gibbs free energy contribution and it should be emphasized that, regardless its name, the stiffness matrix contains information pertaining to all the considered fields and not just to the mechanical field. If a static analysis is required, the system to solve is the following:

$$\boldsymbol{K}\boldsymbol{R} = \boldsymbol{P}. \tag{30}$$

where $\boldsymbol{P}$ is the vector of nodal loads, $\boldsymbol{R}$ is the vector of nodal unknowns.

NUMERICAL RESULTS AND DISCUSSION

A simply supported laminate of two layers of elastic material with two additional piezoelectric layers bonded to the upper and lower surfaces is considered in the following electromechanical case study. Several FEM results are compared with the exact solution provided by Heyliger (1994b) for the [0/90] case (stacking sequence starts from the top). Moreover, the influence of different lamination angles of the two inner layers is accounted for. Results of the [0/0], [15/−15], [30/−30] and [45/−45] stacking sequence are compared for both actuator and sensor configuration. The plate is square with side length a. The total thickness is h. Each elastic layer has a thickness of $0.4\,h$, while the thickness of each piezoelectric layer is $0.1\,h$. The plate aspect ratio is $a/h = 4$. The elastic material is modeled as a fiber-reinforced composite and has the following properties: $E_{11} = 132.38$ (all in GPa); $E_{22} = 10.756$; $E_{33} = 10.756$; $G_{44} = 3.606$; $G_{55} = 5.654$; $G_{66} = 5.654$; $\nu_{12} = 0.24$; $\nu_{13} = 0.24$; $\nu_{23} = 0.49$; $\varepsilon_{11}/\varepsilon_0 = 3.5$ and $\varepsilon_{22}/\varepsilon_0 = \varepsilon_{33}/\varepsilon_0 = 3.0$. The material of the piezoelectric layers is PZT-4, with the following material properties: $E_{11} = E_{22} = 81.3$ (all in GPa); $E_{33} = 64.5$; $G_{44} = G_{55} = 25.6$; $G_{66} = 30.6$; $\nu_{12} = 0.329$; $\nu_{13} = \nu_{23} = 0.432$; $e_{31} = e_{32} = -5.20$ (all in C/m^2); $e_{33} = 15.08$; $e_{24} = e_{15} = 12.72$; $\varepsilon_{11}/\varepsilon_0 = \varepsilon_{11}/\varepsilon_0 = 1475$ and $\varepsilon_{33}/\varepsilon_0 = 1300$. The piezoelectric layer thickness is taken as 0.1 m. Both sensor and actuator cases are considered in the following (the two configuration are illustrated in Figure 1, where p_z indicates a pressure N/m^2 and ϕ_t indicates the potential V imposed on the top face and $\widehat{p}_z = \widehat{\phi}_t = 1$). Concerning boundary conditions, u_z, σ_{zz} and D_z are set to zero at the four edges of the plate; u_x and σ_{xz} are zero along the edges parallel to the y-axis while u_y and σ_{yz} are zero along the edges parallel to the x-axis. The FEM results are obtained with a regular 10×10 mesh of LD2 (or LM2) Q4 FEs to minimize computational costs keeping a good accuracy. This work is mainly focused on the calculation of D_z, which being an intensive variable converges with more difficulties than displacements. The convergence study for the D_z quantity in sensor configuration is illustrated in Figure 2. The analysis is restricted to the LW modeling which is capable to furnish reliable results at each layer interfaces.

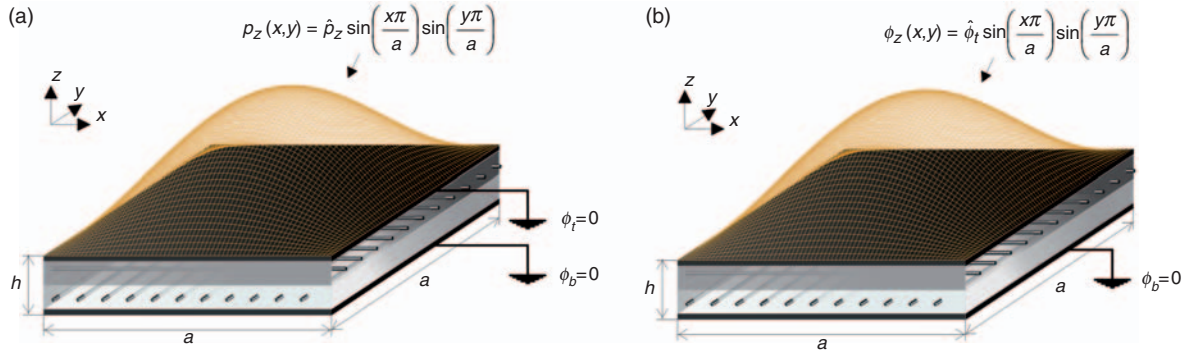

Figure 1. *(a) The plate in sensor configuration (applied pressure); (b) The plate in actuator configuration (applied potential).*

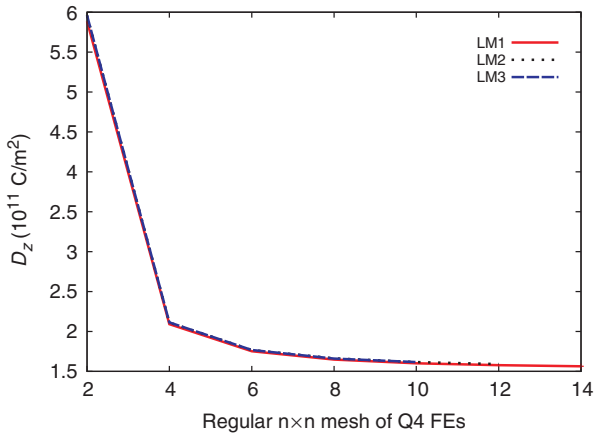

Figure 2. *Convergence study of the electric displacement quantity. Some points are missing for computational reasons.*

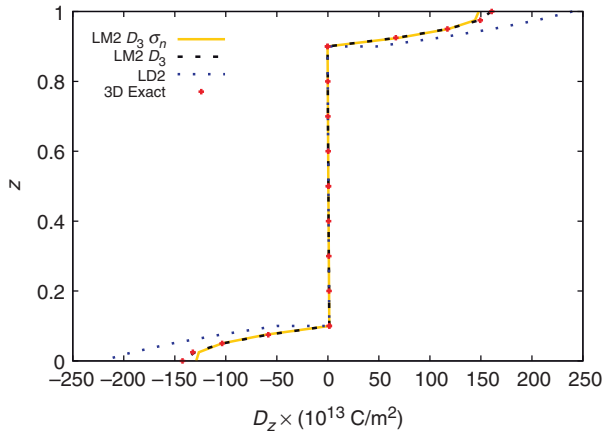

Figure 3. *Sensor case: Comparison between FEM results and 3D-exact solution; the electric displacement is in* C/m^2*; $D_3 = D_3(a/2, b/2)$.*

Discontinuity in electric displacement is not considered in this article (it could be handled doubling the DOFs at the layer interfaces and taking it into account during the assembly procedure). A second order thickness expansion is considered to properly calculate the through-the-thickness electric displacement, which clearly shows a parabolic-like trend through the external layers (Figure 3).

Sensor Case

The applied double sinusoidal pressure loading p_z is considered on the top plate surface (sensor configuration). The load amplitude is equal to 1 N/m^2. The top and bottom laminate surfaces are fixed at zero potential. The exact midplane transverse displacement at the center of the plate is 30.027×10^{-10} m, while the value calculated by the LD2 or LM2 FEs is 30.119×10^{-10} m. Additional comparisons between the exact solution (Heyliger, 1994b) and the FEM results are shown in Tables 1–3 and in Figures 3 and 4.

A comparison between the 3D-exact solution, PVD, RMVT-D_z and RMVT-D_z-σ_n results is provided in Table 1 for displacement u_y and the electric potential ϕ: results of PVD, RMVT-D_z and RMVT-D_z-σ_n modeling are all very close and they are in good agreement with the exact solution (see also Figures 3 and 4). In other words, when D_z is modeled by RMVT, the calculated primary variables do not change significantly with respect to PVD. However, if a slight difference is detected, the RMVT results are closer to the exact solution, RMVT-D_z-σ_n is even slightly more accurate than RMVT-D_z.

A comparison between the 3D-exact solution, PVD and RMVT results is provided in Table 2 for the

Table 1. Sensor case: PVD, RMVT-D_z and RMVT-D_z-σ_n results: Comparison of LD2 and LM2 FEM solutions with the Heyliger 3D-exact solution. Displacements are in* m*; electric potential is in* V*. $u_y = u_y(a/2, 0)$; $\phi = \phi(a/2, b/2)$.

Height	$u_y \times 10^{12}$ 3D	$u_y \times 10^{12}$ RMVT-D_z-σ_n	$u_y \times 10^{12}$ RMVT-D_z	$u_y \times 10^{12}$ PVD	$\phi \times 10^{1}$ 3D	$\phi \times 10^{1}$ RMVT-D_z-σ_n	$\phi \times 10^{1}$ RMVT-D_z	$\phi \times 10^{1}$ PVD
1.000	−47.549	−45.893	−45.594	−45.593	0.0000	0.0000	0.0000	0.0000
0.975	−41.425	−39.850	−39.528	−39.527	0.0189	0.0183	0.0181	0.0181
0.950	−35.424	−33.891	−33.569	−33.567	0.0358	0.0340	0.0336	0.0336
0.925	−29.531	−28.016	−27.772	−27.715	0.0488	0.0470	0.0464	0.0464
0.900	−23.732	−22.225	−21.970	−21.969	0.0598	0.0575	0.0567	0.0567
0.800	−10.480	−10.375	−10.577	−10.058	0.0589	0.0567	0.0559	0.0560
0.700	0.1413	0.1555	−0.0836	−0.0836	0.0589	0.0567	0.0559	0.0560
0.600	9.8917	9.3673	9.5108	9.5104	0.0596	0.0575	0.0567	0.0567
0.500	20.392	17.260	18.206	18.205	0.0611	0.0590	0.0583	0.0583
0.400	24.768	22.282	22.150	22.149	0.0634	0.0613	0.0605	0.0606
0.300	29.110	27.448	26.703	26.700	0.0665	0.0645	0.0637	0.0637
0.200	33.819	32.756	31.863	31.860	0.0706	0.0685	0.0677	0.0677
0.100	39.309	38.208	37.632	37.628	0.0756	0.0734	0.0726	0.0726
0.075	44.492	43.548	42.934	42.930	0.0602	0.0587	0.0581	0.0581
0.050	49.772	48.979	48.346	48.341	0.0425	0.0415	0.0411	0.0411
0.025	55.163	54.503	53.867	53.863	0.0224	0.0220	0.0218	0.0218
0.000	60.678	60.118	59.499	59.494	0.0000	0.0000	0.0000	0.0000

Table 2. Sensor case: PVD, RMVT-D_z and RMVT-D_z-σ_n results, comparison of LD2 and LM2 FEM solutions with the Heyliger 3D-exact solution. Stresses are in* Pa. $\sigma_{zz}=\sigma_{zz}(a/2, b/2)$; $\sigma_{xx}=\sigma_{xx}(a/2, b/2)$.

Height	$\sigma_{zz}\times 10^1$ 3D	$\sigma_{zz}\times 10^1$ RMVT-D_z-σ_n	$\sigma_{zz}\times 10^1$ RMVT-D_z	$\sigma_{zz}\times 10^1$ PVD	σ_{xx} 3D	σ_{xx} RMVT-D_z-σ_n	σ_{xx} RMVT-D_z	σ_{xx} PVD
1.000	10.000	10.409	9.6381	9.6313	6.5643	6.2798	6.2387	6.2392
0.975	9.9657	10.282	9.4354	9.4336	5.8201	5.5511	5.5030	5.5033
0.950	9.8682	10.164	9.3598	9.3631	5.0855	4.8373	4.7856	4.7857
0.925	9.7154	10.053	9.4112	9.4197	4.3595	4.1385	4.0866	4.0865
0.900	9.5151	9.9506	9.5898	9.6034	3.6408	3.4547	3.4059	3.4057
0.900	9.5151	9.9506	10.163	10.163	2.8855	3.8732	3.8362	3.8364
0.800	8.5199	8.7869	8.7018	8.7018	1.4499	1.9801	2.0093	2.0094
0.700	7.3747	7.6086	7.4395	7.4395	0.2879	0.3008	0.3332	0.3332
0.600	6.1686	6.4158	6.3764	6.3764	−0.7817	−1.1648	−1.1922	−1.1923
0.500	4.9831	5.2084	5.5124	5.5124	−1.9266	−2.4166	−2.5669	−2.5670
0.500	4.9831	5.2084	4.9179	4.9178	0.0991	0.0522	0.0527	0.0527
0.400	3.8045	3.8671	3.9244	3.9244	−0.0149	−0.0773	−0.0683	−0.0683
0.300	2.6137	2.6395	2.8259	2.8259	−0.1280	−0.2168	−0.2049	−0.2049
0.200	1.4821	1.5255	1.6223	1.6223	−0.2426	−0.3664	−0.3570	−0.3571
0.100	0.4868	0.5251	0.3136	0.3136	−0.3616	−0.5260	−0.5247	−0.5248
0.100	0.4868	0.5251	0.8365	0.8251	−4.2348	−4.0013	−3.9325	−3.9325
0.075	0.2845	0.2641	0.9436	0.9872	−4.8806	−4.6334	−4.5634	−4.5636
0.050	0.1312	0.1006	1.0339	1.0311	−5.5337	−5.2799	−5.2119	−5.2123
0.025	0.0340	0.0344	0.9553	0.9568	−6.1951	−5.9409	5.8780	−5.8785
0.000	0.0000	0.0657	0.7583	0.7641	−6.8658	−6.6163	−6.5617	−6.5623

Table 3. Sensor case: Comparison of FEM and Heyliger 3D-exact solutions, LD2 and LM2 FEs are employed for PVD and RMVT case, respectively. The electric displacement is in* C/m^2; $D_z=D_z(a/2, b/2)$.

Height	$D_z\times 10^{13}$ 3D	RMVT-D_z-σ_n	RMVT-D_z	PVD
1.000	160.58	147.89	160.22	239.57
0.975	149.35	144.14	148.27	204.92
0.950	117.23	118.20	117.53	161.38
0.925	66.568	70.044	68.003	108.95
0.900	−0.3382	−0.311	−0.3044	47.621
0.900	−0.3382	−0.311	−0.3044	−0.2990
0.800	−0.1276	−0.105	−0.0969	−0.0977
0.700	0.0813	0.099	0.1064	0.1037
0.600	0.2913	0.303	0.3058	0.3051
0.500	0.5052	0.505	0.5010	0.5065
0.500	0.5052	0.505	0.5010	0.4943
0.400	0.7259	0.725	0.7228	0.7236
0.300	0.9563	0.953	0.9495	0.9529
0.200	1.1995	1.189	1.1812	1.1821
0.100	1.4587	1.433	1.4179	1.4114
0.100	1.4587	1.433	1.4179	−50.162
0.075	−58.352	−61.217	−59.178	−105.53
0.050	−103.66	−103.84	−103.15	−152.63
0.025	−132.40	−126.43	−130.50	−191.45
0.000	−142.46	−128.99	−141.23	−222.00

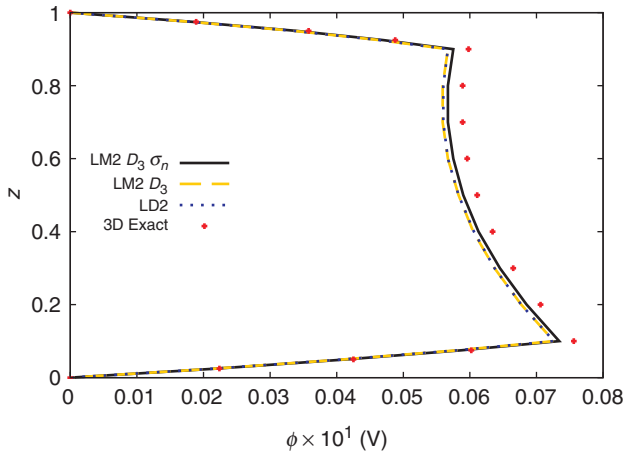

***Figure 4.** Sensor case: Comparison between FEM results and 3D-exact solution; electric potential is in* V; $\phi=\phi(a/2, b/2)$.

transverse stress σ_{zz} and for the in-plane stresses σ_{yy} and σ_{xy}: all results of the in-plane stresses are close to the exact solutions. It has been confirmed that, even for in-plane stresses, the difference between PVD, RMVT-D_z and RMVT-D_z-σ_n is negligible. At the contrary, only the RMVT-D_z-σ_n modeling provides the continuity of the transverse stress σ_{zz} at the layer-interfaces. It can be noted that, concerning the bottom layer, the results of σ_{zz} obtained employing the RMVT-D_z-σ_n modeling are significantly closer to the 3D solution than those obtained with the PVD or RMVT-D_z modeling. The advantage of the RMVT-D_z-σ_n application when calculating the transverse stresses is confirmed in the following section also for the actuator case.

The accuracy of both of the presented RMVT models is evident in Table 3, where the evaluation of transverse electric displacement is referred to. The results are compared to the 3D-exact and the PVD solutions. It should be underlined that RMVT-D_z and RMVT-D_z-σ_n lead to

Table 4. Sensor case: RMVT-D_z-σ_n, LM2 results for different lamination angles. Electric potential is in V, transverse electric displacement is in C/m^2. $\phi = \phi(a/2, b/2)$; $D_z = D_z(a/2, b/2)$.

Height	$\phi \times 10$ [0°/0°]	$\phi \times 10$ [15°/−15°]	$\phi \times 10$ [30°/−30°]	$\phi \times 10$ [45°/−45°]	$D_z \times 10^{13}$ [0°/0°]	$D_z \times 10^{13}$ [15°/−15°]	$D_z \times 10^{13}$ [30°/−30°]	$D_z \times 10^{13}$ [45°/−45°]
1.000	0.0000	0.0000	0.0000	0.0000	133.9	135.5	133.4	128.9
0.980	0.0131	0.0133	0.0132	0.0130	133.1	135.7	135.4	132.0
0.960	0.0246	0.0250	0.0249	0.0245	119.3	122.2	123.1	120.7
0.940	0.0345	0.0351	0.0349	0.0344	92.48	95.06	96.32	94.81
0.920	0.0428	0.0436	0.0433	0.0426	52.69	54.28	55.22	54.50
0.900	0.0495	0.0505	0.0502	0.0493	−0.0984	−0.1682	−0.2548	−0.2829
0.900	0.0495	0.0505	0.0502	0.0493	−0.0984	−0.1682	−0.2548	−0.2829
0.820	0.0494	0.0502	0.0496	0.0487	0.0462	−0.0192	−0.1051	−0.1369
0.740	0.0498	0.0503	0.0495	0.0485	0.1906	0.1296	0.0440	0.0086
0.660	0.0506	0.0509	0.0499	0.0487	0.3349	0.2780	0.1927	0.1536
0.580	0.0518	0.0520	0.0507	0.0494	0.4791	0.4262	0.3409	0.2982
0.500	0.0535	0.0535	0.0520	0.0505	0.6231	0.5741	0.4887	0.4422
0.500	0.0535	0.0535	0.0520	0.0505	0.6231	0.5741	0.4887	0.4422
0.420	0.0556	0.0555	0.0537	0.0521	0.7845	0.7374	0.6489	0.5975
0.340	0.0582	0.0580	0.0559	0.0541	0.9511	0.9057	0.8137	0.7570
0.260	0.0613	0.0610	0.0586	0.0566	1.123	1.079	0.983	0.921
0.180	0.0650	0.0645	0.0618	0.0597	1.300	1.258	1.157	1.088
0.100	0.0691	0.0685	0.0655	0.0632	1.482	1.441	1.336	1.260
0.100	0.0691	0.0685	0.0655	0.0632	1.482	1.441	1.336	1.260
0.080	0.0582	0.0578	0.0554	0.0535	−47.20	−48.00	−47.52	−45.89
0.060	0.0459	0.0456	0.0438	0.0423	−83.85	−84.84	−83.28	−80.02
0.040	0.0321	0.0319	0.0307	0.0297	−108.5	−109.1	−105.9	−101.1
0.020	0.0168	0.0167	0.0161	0.0156	−121.1	−120.7	−115.5	−109.2
0.000	0.0000	0.0000	0.0000	0.0000	−121.7	−119.8	−112.0	−104.3

an almost 3D-exact description of D_z, while PVD results can be affected by very large errors (see also Figure 3).

In Table 4 the results of electric potential and transverse electric displacement are presented for different lamination angles. The maximum electric potential depends on the stacking sequence. The distribution of the potential along thickness is also shown in Figure 5. Also the electric displacement clearly depends on the chosen lamination angle, see Table 4.

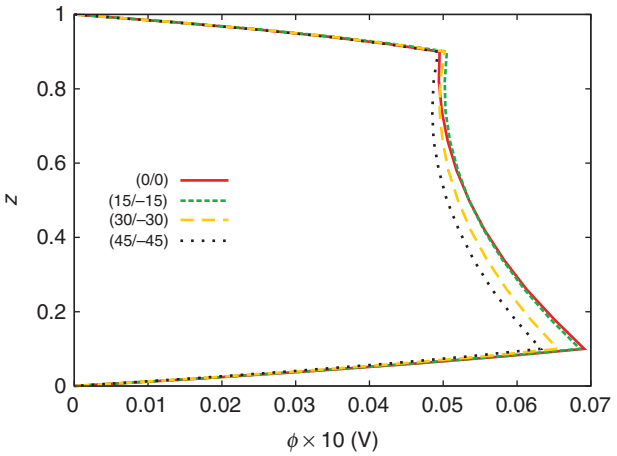

Figure 5. *Sensor case: Electric potential ϕ for different lamination angles; RMVT-D_z-σ_n LM2 model; $\phi = \phi(a/2, b/2)$.*

Actuator Case

The applied double sinusoidal potential p_z is considered at the top plate surface (actuator configuration). The load amplitude is equal to 1 V and the bottom laminate surface is fixed at zero potential. The exact midplane transverse displacement at the center of the plate is -14.711×10^{-12} m, while the value calculated by LD2 and LM2 FEs are -14.151×10^{-12} m and -14.152×10^{-12} m, respectively. Other comparisons between the exact solution (Heyliger, 1994b) and the FEM results are shown in Tables 5–8.

The following remarks can be made. Table 5 shows that the FEM results of primary variables u_y and ϕ, are in good agreement with the exact solution provided by Heyliger (1994b). As far as Table 6 is concerned, the in-plane stresses are also calculated with good accuracy. Normal stress σ_{zz} does not have reasonable values around the plate top and the bottom face when PVD or RMVT-D_z modeling is addressed to. If the through-the-thickness expansion is refined to the third order, RMVT-D_z-σ_n leads to good results of σ_{zz} even around the top and the bottom area of the plate, while PVD and RMVT-D_z results still remains out of range, see Table 7 and Figure 6. From Table 8 it is clear that the RMVT-D_z modeling does not significantly improve the solution of the actuator case if compared to the PVD modeling. In Table 9 the through-the-thickness distributions of the transverse displacement u_z and in-plane

Table 5. Actuator case: PVD, RMVT-D_z and RMVT-D_z-σ_n results: comparison of LD2 and LM2 FEM solutions with the 3D Heyliger solution. Displacements are in m*; electric potential is in* V*. $u_y = u_y(a/2, 0)$; $\phi = \phi(a/2, b/2)$.*

Height	$u_y \times 10^{12}$ 3D	$u_y \times 10^{12}$ RMVT-D_z-σ_n	$u_y \times 10^{12}$ RMVT-D_z	$u_y \times 10^{12}$ PVD	ϕ 3D	ϕ RMVT-D_z-σ_n	ϕ RMVT-D_z	ϕ PVD
1.000	−32.764	−33.442	−33.951	−33.951	1.0000	1.0000	1.0000	1.0000
0.975	−23.349	−24.014	−24.377	−24.377	0.9971	0.9972	0.9972	0.9972
0.950	−13.973	−14.619	−14.826	−14.826	0.9950	0.9951	0.9951	0.9951
0.925	−4.6174	−5.2570	−5.2977	−5.2983	0.9936	0.9936	0.9936	0.9936
0.900	4.7356	4.0721	4.2069	4.2064	0.9929	0.9929	0.9929	0.9929
0.800	2.9808	2.4479	2.5448	2.5445	0.8415	0.8422	0.8422	0.8423
0.700	1.7346	1.2092	1.2548	1.2546	0.7014	0.7011	0.7011	0.7011
0.600	0.8008	0.3560	0.3368	0.3368	0.5707	0.5695	0.5695	0.5695
0.500	0.0295	−0.1117	−0.2091	−0.2091	0.4476	0.4475	0.4475	0.4473
0.400	−0.4404	−0.5571	−0.5745	−0.5745	0.3305	0.3311	0.3311	0.3310
0.300	−0.8815	−0.9741	−0.9517	−0.9518	0.2179	0.2177	0.2177	0.2177
0.200	−1.3206	−1.3625	−1.3408	−1.3409	0.1081	0.1073	0.1073	0.1073
0.100	−1.7839	−1.7223	−1.7418	−1.7419	−0.0001	−0.0001	−0.0001	−0.0001
0.075	−2.0470	−1.9735	−1.9963	−1.9963	−0.00009	−0.0001	−0.00009	−0.00009
0.050	−2.3140	−2.2278	−2.2554	−2.2554	−0.00008	−0.0001	−0.00007	−0.00007
0.025	−2.5856	−2.4852	−2.5191	−2.5191	−0.00004	−0.00004	−0.00004	−0.00004
0.000	−2.8625	−2.7455	−2.7876	−2.7875	0.00000	0.00000	0.00000	0.00000

Table 6. Actuator case: PVD, RMVT-D_z and RMVT-D_z-σ_n results: comparison of LD2 and LM2 FEM solutions with the 3D Heyliger solution. Stresses are in Pa*. $\sigma_{zz} = \sigma_{zz}(a/2, b/2)$; $\sigma_{xx} = \sigma_{xx}(a/2, b/2)$.*

Height	$\sigma_{zz} \times 10^3$ 3D	$\sigma_{zz} \times 10^3$ RMVT-D_z-σ_n	$\sigma_{zz} \times 10^3$ RMVT-D_z	$\sigma_{zz} \times 10^3$ PVD	$\sigma_{xx} \times 10^2$ 3D	$\sigma_{xx} \times 10^2$ RMVT-D_z-σ_n	$\sigma_{xx} \times 10^2$ RMVT-D_z	$\sigma_{xx} \times 10^2$ PVD
1.000	0.0000	−3.9972	−55.419	−55.800	111.81	108.42	113.26	113.28
0.975	−0.8333	−0.3973	−43.183	−43.279	63.736	62.944	66.175	66.186
0.950	−2.8471	−0.7247	−28.574	−28.385	15.833	17.986	19.447	19.448
0.925	−5.3241	−4.9793	−11.592	−11.118	−32.001	−26.455	−26.923	−26.932
0.900	−7.5482	−13.161	−7.7627	−8.5218	−79.865	−70.380	−72.935	−72.955
0.900	−7.5482	−13.161	−15.581	−15.579	−51.681	−65.888	−68.104	−68.096
0.800	−12.957	−12.947	−11.569	−11.567	−33.135	−40.198	−41.753	−41.748
0.700	−15.245	−14.028	−11.714	−11.713	−19.840	−20.629	−21.345	−21.342
0.600	−15.510	−16.402	−16.016	−16.014	−9.7737	−7.1803	−6.8808	−6.8792
0.500	−14.612	−20.070	−24.475	−24.473	−1.3905	0.1477	1.6397	1.6408
0.500	−14.612	−20.070	−17.337	−17.335	−1.3089	−1.2422	−1.2975	−1.2973
0.400	−12.524	−12.273	−12.939	−12.937	−0.5782	−0.2467	−3.3091	−3.3075
0.300	−9.2558	−7.3716	−9.2096	−9.2086	0.1348	0.6476	5.7872	5.7883
0.200	−5.5018	−5.3653	−6.1495	−6.1487	0.8463	1.4408	1.4313	1.4314
0.100	−1.8733	−6.2545	−3.7583	−3.7579	1.5723	2.1326	2.2270	2.2270
0.100	−1.8733	−6.2545	−2.8333	−3.3555	14.529	13.973	13.988	14.007
0.075	−1.1074	−0.4685	−3.7838	−4.1098	17.801	16.911	17.030	17.041
0.050	−0.5162	1.7426	−4.2493	−4.3795	21.098	19.895	20.144	20.148
0.025	−0.1351	0.3790	−4.2299	−4.1645	24.428	22.927	23.331	23.328
0.000	0.0000	−4.5594	−3.7256	−3.4647	27.795	26.006	26.591	26.581

stress σ_{xx} are presented for various lamination angles. All the results are obtained with the RMVT-D_z-σ_n modeling. Figure 7 points out the dependency of u_z on the lamination angle. Also the transverse stress σ_{zz} at center of the plate is shown in the same figure for different stacking sequences. It can be noted that increasing the lamination angles from [0/0] to [45/−45] leads to lower values of transverse displacement. On the contrary, the stresses can increase significantly for very anisotropic cases.

Computational Effort

The three different FEs illustrated in this work are obtained via the application of the PVD, RMVT-D_z and RMVT-D_z-σ_n modeling. If n^2 is the number of DOFs, involved in the PVD analysis, RMVT-D_z and RMVT-D_z-σ_n modeling would require $(n+1)^2$ and $(n+4)^2$ DOFs, respectively. To be underlined that, using reasonable meshes, the different accuracy in the FEM solution is due to the application of different

Table 7. Actuator case: Comparison between FEM solutions and 3D Heyliger solution for σ_{zz}; LM3 model is employed. Stresses are in Pa. $\sigma_{zz}=\sigma_{zz}(a/2, b/2)$.

Height	$\sigma_{zz}\times 10^3$ 3D	$\sigma_{zz}\times 10^3$ RMVT-D_z-σ_n (LM3)	$\sigma_{zz}\times 10^3$ RMVT-D_z (LM3)	$\sigma_{zz}\times 10^3$ PVD (LD3)
1.000	0.0000	0.4571	−57.905	−58.103
0.975	−0.8333	−1.0703	−43.104	−43.032
0.950	−2.8471	−2.9855	−26.449	−26.352
0.925	−5.3241	−5.4381	−10.137	−10.260
0.900	−7.5482	−8.5777	3.6320	3.0439
0.900	−7.5482	−8.5777	−8.5081	−8.5069
0.800	−12.957	−13.923	−12.543	−12.541
0.700	−15.245	−16.470	−16.157	−16.155
0.600	−15.510	−16.706	−17.288	−17.286
0.500	−14.612	−15.120	−13.873	−13.871
0.500	−14.612	−15.120	−16.929	−16.927
0.400	−12.524	−13.404	−13.102	−13.101
0.300	−9.2558	−9.6210	−10.022	−10.021
0.200	−5.5018	−5.3821	−6.4388	−6.4380
0.100	−1.8733	−2.2994	−1.0987	−1.0986
0.100	−1.8733	−2.2994	−4.3942	−4.4100
0.075	−1.1074	−0.8874	−4.0307	−4.0339
0.050	−0.5162	−0.5092	−3.9599	−3.9570
0.025	−0.1351	−0.3347	−4.1049	−4.1027
0.000	0.0000	0.4661	−4.3889	−4.3942

Table 8. Actuator case: Comparison between FEM results, LD2 and LM2 FEs are employed for PVD and RMVT case, respectively. The electric displacement is in C/m^2. $D_z=D_z(a/2, b/2)$.

Height	$D_z\times 10^{13}$ RMVT-D_z-σ_n	RMVT-D_z	PVD
1.000	−243.62	−244.31	−243.82
0.975	−183.67	−184.16	−183.88
0.950	−123.78	−124.08	−123.95
0.925	−63.930	−64.070	−64.043
0.900	−4.1326	−4.1321	−4.1504
0.900	−4.1326	−4.1321	−4.1274
0.800	−3.8750	−3.8746	−3.8751
0.700	−3.6209	−3.6205	−3.6228
0.600	−3.3703	−3.3700	−3.3705
0.500	−3.1233	−3.1229	−3.1182
0.500	−3.1233	−3.1229	−3.1275
0.400	−3.0501	−3.0498	−3.0492
0.300	−2.9735	−2.9732	−2.9709
0.200	−2.8934	−2.8931	−2.8925
0.100	−2.8099	−2.8095	−2.8142
0.100	−2.8099	−2.8095	−2.8425
0.075	−2.8400	−2.8409	−2.8144
0.050	−2.8387	−2.8384	−2.7898
0.025	−2.8059	−2.8020	−2.7685
0.000	−2.7418	−2.7316	−2.7507

variational statements. From numerical results showed in this section it is clear that the PVD provides accurate numbers for displacements, in-plane stresses and the electric potential. In addition to PVD, the RMVT-D_z calculates with high accuracy the electric displacement, while if accurate normal stresses values are required too, the RMVT-D_z-σ_n is the appropriate modeling to be used. To be more rigorous, an extreme mesh refinement of PVD FEs would provide good results also for transverse stresses and electric displacement, but the use of RMVT assures the same accuracy without any additional mesh refinement that would not make possible the analysis for computational reasons.

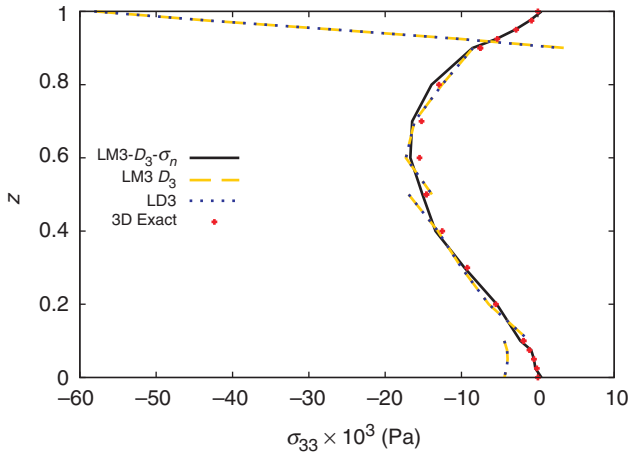

Figure 6. *Actuator case: Comparison of FEM results and 3D-exact solution; the transverse normal stress σ_{zz} is in* Pa*; $\sigma_{zz}=\sigma_{zz}(a/2, b/2)$.*

CONCLUSIONS

An extended mixed variational statement (RMVT-D_z-σ_n) is proposed in this work for the *a priori* evaluation of the transverse electric displacement D_z and transverse stresses σ_n at the same time. Advanced plate FEs have been developed to asses the numerical performance of RMVT-D_z-σ_n. For orthotropic and anisotropic plates, the numerical results clearly show that RMVT-D_z-σ_n is capable of furnishing almost the 3D-results of D_z. Concerning the sensor case, worse evaluations of D_z are instead obtained by using the PVD variational statement, which discard the IC of D_z. In addition, to the RMVT-D_z-σ_n application, also the transverse stresses are calculated with high accuracy. It is showed that a slightly different variational statement called RMVT-D_z, is applicable when accurate results are needed only for D_z and not for σ_n. In conclusion, the RMVT-D_z-σ_n should be preferred to other variational statements when fast and accurate results are needed for the prediction of both σ_n and D_z quantities (D_z is essential for the evaluation of the electrical charge Q on the plate).

Table 9. Actuator case: RMVT-D_z-σ_n FEM results for different lamination angles. Displacements are in m, stresses are in Pa. $u_z = u_z(a/2, b/2)$; $\sigma_{xx} = \sigma_{xx}(a/2, b/2)$.

Height	$u_z \times 10^{13}$ [0°/0°]	$u_z \times 10^{13}$ [15°/−15°]	$u_z \times 10^{13}$ [30°/−30°]	$u_z \times 10^{13}$ [45°/-45°]	$\sigma_{xx} \times 10^2$ [0°/0°]	$\sigma_{xx} \times 10^2$ [15°/−15°]	$\sigma_{xx} \times 10^2$ [30°/−30°]	$\sigma_{xx} \times 10^2$ [45°/−45°]
1.000	−139.3	−140.3	−139.0	−137.4	109.0	110.1	114.9	115.0
0.980	−130.8	−131.7	−130.3	−128.7	72.34	73.39	76.97	76.98
0.960	−124.4	−125.3	−123.8	−122.1	35.99	37.05	39.25	39.25
0.940	−120.2	−121.0	−119.4	−117.6	−0.031	1.063	1.776	1.771
0.920	−118.0	−118.7	−117.1	−115.2	−35.72	−34.59	−35.46	−35.47
0.900	−117.9	−118.6	−116.9	−115.0	−71.09	−69.90	−72.44	−72.47
0.900	−117.9	−118.6	−116.9	−115.0	−64.22	−60.14	−62.25	−62.25
0.820	−120.9	−121.4	−119.3	−117.1	−44.66	−41.30	−42.65	−42.64
0.740	−123.3	−123.6	−121.0	−118.6	−29.10	−26.13	−26.83	−26.83
0.660	−125.1	−125.2	−122.2	−119.5	−17.54	−14.63	−14.80	−14.80
0.580	−126.2	−126.1	−122.7	−119.8	−9.965	−6.815	−6.553	−6.552
0.500	−126.8	−126.5	−122.6	−119.5	−6.388	−2.675	−2.094	−2.093
0.500	−126.8	−126.5	−122.6	−119.5	−5.798	−9.720	−10.22	−10.22
0.420	−127.5	−126.9	−122.5	−119.2	−1.616	−4.331	−4.600	−4.599
0.340	−128.0	−127.1	−122.3	−118.8	3.244	1.209	1.144	1.145
0.260	−128.3	−127.1	−122.0	−118.4	8.781	6.899	7.011	7.012
0.180	−128.3	−126.9	−121.5	−117.8	15.00	12.74	13.00	13.00
0.100	−128.1	−126.5	−120.9	−117.1	21.89	18.73	19.11	19.11
0.100	−128.1	−126.5	−120.9	−117.1	7.864	9.625	9.668	9.686
0.080	−127.9	−126.3	−120.7	−116.9	10.13	11.85	11.95	11.96
0.060	−127.7	−126.1	−120.5	−116.7	12.41	14.08	14.26	14.27
0.040	−127.5	−125.9	−120.2	−116.4	14.70	16.33	16.61	16.62
0.020	−127.2	−125.6	−119.9	−116.1	16.99	18.60	19.00	19.00
0.000	−127.0	−125.3	−119.6	−115.7	19.30	20.88	21.43	21.42

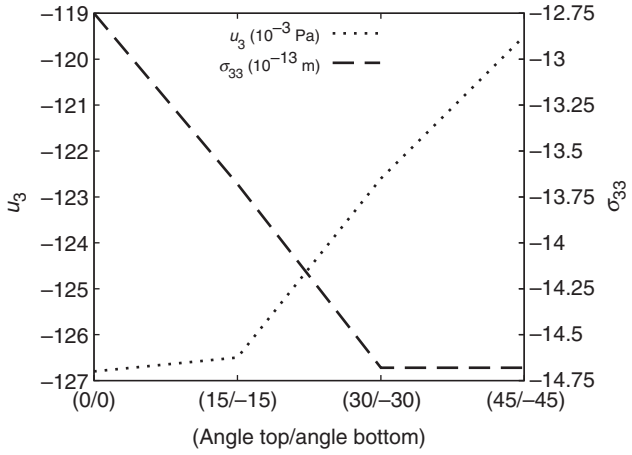

Figure 7. *Actuator case: Midplane transverse displacement* u_z *and transverse normal stress* σ_{zz} *for different lamination angles; RMVT-*D_z*-*σ_n *LM3 modeling;* $\sigma_{zz} = \sigma_{zz}(a/2, b/2)$; $u_z = u_z(a/2, b/2)$.

ACKNOWLEDGMENT

This work has been partially carried out in the framework of Piemonte Regional Project STEP.

REFERENCES

Allik, E. and Hughes, T.J.R. 1970. "Finite Element Method for Piezoelectric Vibration," *International Journal for Numerical Methods in Engineering*, 2:151–157.

Ambartsumian, S.A. 1958. "On a Theory of Bending of Anisotropic Plate," *Investiia Akad Nauk SSSR, Ot Tekh Nauk:* 4.

Auricchio, F., Bisegna, P. and Lovadina, C. 2001. "Finite Element Approximation of Piezoelectric Plates," *International Journal for Numerical Methods in Engineering*, 50:1469–1499.

Ballhause, D., D'Ottavio, M., Kröplin, B. and Carrera, E. 2004. "A Unified Formulation to Assess Multilayered Theories for Piezoelectric Plates," *Computers and Structures*, 83: 1217–1235.

Benjeddou, A. 2000. "Advances in Piezoelectric Finite Element Modeling of Adaptive Structural Elements: A Survey," *Computers and Structures*, 76:347–363.

Benjeddou, A. and Andrianarison, O. 2005. "Unified Partial Mixed Variational Formulations for Heat Transfer and Thermal Stress Dynamic Coupled Responses of Multilayer Composites," *Mechanics of advanced Materials and Structures*, 12:1–11.

Carrera, E. 1995. "A Class of Two Dimensional Theories for Multilayered Plates Analysis," *Atti Accademia delle Scienze di Torino, Memorie Scienze Fisiche*, 19–20:49–87.

Carrera, E. 1996. "C_z^o Reissner-Mindlin Multilayered Plate Elements Including Zig-Zag and Interlaminar Stresses Continuity," *International Journal for Numerical Methods in Engineering*, 39:1797–1820.

Carrera, E. 1997. "An Improced Reissner-Mindlin Type Element for the Electromechanical Analysis of Multilayered Plates Including

Piezo Layers,'' *Journal of Intelligent Material Systems and Structures*, 8:232–248.

Carrera, E. 1998. ''Evaluation of Layer-wise Mixed Theories for Laminated Plates Analysis,'' *AIAA Journal*, 36:830–839.

Carrera, E. 1999a. ''A Reissner's Mixed Variational Theorem Applied to Vibrational Analysis of Multilayered Shell,'' *Journal of Applied Mechanics*, 66:69–68.

Carrera, E. 1999b. ''A Study of Transverse Normal Stress Effects on Vibration of Multilayered Plates and Shells,'' *Journal of Applied Mechanics*, 225:803–829.

Carrera, E. 2000. ''Single Layer vs Multilayer Plate Modelings on the Base of Reissner's Mixed Theorem,'' *AIAA Journal*, 38: 342–352.

Carrera, E. 2001. ''Developments, Ideas and Evaluations Based upon the Reissner's Mixed Theorem in the Modeling of Multilayered Plates and Shells,'' *Applied Mechanics Review*, 54:301–329.

Carrera, E. 2003a. ''Historical Review of Zig-Zag Theories for Multilayered Plates and Shells,'' *Applied Mechanics Review*, 56:287–308.

Carrera, E. 2003b. ''Theories and Finite Elements for Multilayered Plates and Shells: A Unified Compact Formulation with Numerical Assessment and Benchmarking,'' *Archives of Computational Method in Engineering*, 10:215–296.

Carrera, E., Brischetto, S. and D'Ottavio, M. 2005. ''Vibrations of Piezoelectric Shells by Unified Formulations in the Reissner's Mixed Theorem,'' In: *II Eccomas Thematic Conference on Smart Structures and Materials*, Lisbon.

Carrera, E. and Boscolo, M. 2007. ''Classical and Mixed Finite Elements for Static and Dynamics Analysis of Piezoelectric Plates,'' *International Journal for Numerical Methods in Engineering*, 70:253–291.

Carrera, E. and DeMasi, L. 2002a. ''Classical and Advanced Multilayered Plate Elements Based upon PVD and RMVT. Part 1. Derivation of Finite Element Matrices,'' *International Journal for Numerical Methods in Engineering*, 55:191–231.

Carrera, E. and DeMasi, L. 2002b. ''Classical and Advanced Multilayered Plate Elements Based upon PVD and RMVT. Part 2. Numerical Implementations,'' *International Journal for Numerical Methods in Engineering*, 55:253–291.

Carrera, E. 2002c. ''Theories and Finite Elements for Multilayered Anisotropic, Composite Plates and Shells,'' *Archives of Computational Methods in Engineering*, 9:87–140.

Carrera, E. and Fagiano, C. 2008a. ''Mixed Piezoelectric Plate Elements with Continuous Transverse Electric Displacements,'' *Journal of Mechanics of Materials and Structures*, 2:421–438.

Carrera, E., Brischetto, S. and Nali, P. 2008b. ''Variational Statements and Computational Models for Mmultifield Problems and Multilayered Structures,'' *Special Issue of MAMS*, 1583: 182–198.

Carrera, E. and Nali, P. 2009. ''Mixed Piezoelectric Plate Elements with Direct Evaluation of Transverse Electric Displacement,'' *International Journal for Numerical Methods in Engineering*, 80:403–424.

Chopra, I. 1996. ''State-of-the-art of Smarts Structures and Integrated Systems,'' In: *SPIE Smart Structures and Materials Conference SPIE*, 2717:20–62.

Chopra, I. 2002. ''Review of State of Art of Smart Structures and Integrated Systems,'' *AIAA Journal*, 40:2145–2187.

D'Ottavio, M. and Kröplin, B. 2006. ''An Extension of Reissner Mixed Variational Theorem to Piezoelectric Laminates,'' *Mechanics of Advanced Materials and Structures*, 13:139–150.

Eer Nisse, E.P. 1967a. ''Variational Method for Electrostatic Vibration Analysis,'' *IEEE Transactions on Ultrasonics*, SU 14:153–160.

Eer Nisse, E.P. 1967b. ''Variational Method for Electroelastic Vibrations Analysis,'' *IEEE Transaction on Sonics and Ultrasonics*, SU-14:153–160.

Garcia Lage, R., Mota Soares, C.M., Mota Soares, C.A. and Reddy, J.N. 2004a. ''Analysis of Adaptive Plate Structures by Mixed Layerwise Finite Element,'' *Composite and Structures*, 66:269–276.

Garcia Lage, R., Mota Soares, C.M., Mota Soares, C.A. and Reddy, J.N. 2004b. ''Modelling of Piezolaminated Plates Using Layerwise Mixed Finite Elements,'' *Computers and Structures*, 82:1849–1863.

Heyliger, P., Ramirez, G. and Saravanos, D. 1994a. ''Coupled Discrete-layr Finite Elements for Laminated Piezoelectric Plates,'' *Communication in Numerical Methods in Engineering*, 10:971–981.

Heyliger, P. 1994b. ''Static Behavior of Laminated Elastic-Piezoelectric Plates,'' *AIAA Journal*, 32:2481–2484.

Kogl, M. and Bucalem, M.L. 2005a. ''Analysis of Smart Laminates Using Piezoelectric Mitc Plate and Shell Elements,'' *Computers and Structures*, 83:1153–1163.

Kogl, M. and Bucalem, M.L. 2005b. ''A Family of Piezoelectric MITC Plate Elements,'' *Computers and Structures*, 83:1277–1297.

Lammering, R. 1991. ''The Application of A Finite Shell Element for Composites Containing Piezo-Electric Polymers in Vibration Control,'' *Computers and Structures*, 41:1101–1109.

Lekhnitskii, S.G. 1935. ''Strength Calculation of Composite Beams,'' *Vestnik inzhen I teknikov*, 9:137–148.

Mindlin, R.D. 1952. ''Forced Thickness-Shear and Flexural Vibrations of Piezoelectric Crystal Plates,'' *Journal of Applied Physics*, 23:83–88.

Mota Soares, C.A., Reddy, J.N., Garcia Lage, R. and Mota Soares, C.M. 2004. ''Layerwise Partial Mixed Finite Element Analysis of Magneto-electro-elastic Plates,'' *Computers and Structures*, 82:1293–1301.

Oh, J. and Cho, M. 2004. ''A Finite Element Based on Cubic Zig-Zag Plate Theory for the Prediction of Thermo-electric-mechanical Behaviors,'' *International Journal of Solids and Structures*, 41:1331–1356.

Reddy, J.N. 1987. ''A Generalization of Two-Dimensional Theories of Laminated Composite Plates,'' *Communications in Applied Numerical Methods*, 3:173–180.

Reddy, J.N. 1999. *Mechanics of Laminated Composite Plates and Shells, Theory and Analysis*, CRC Press, Boca Raton.

Reissner, E. 1984. ''On a Certain Mixed Variational Theory and a Proposed Application,'' *International Journal for Numerical Methods in Engineering*, 20:1366–1368.

Robaldo, A., Carrera, E. and Benjeddou, A. 2006. ''A Unified Formulation for Finite Element Analysis of Piezoelectric Adaptive Plates,'' *Computers and Structures*, 84:1494–1505.

Saravanos, D.A. and Heyliger, P.R. 1999. ''Mechanics and Computational Models for Laminated Piezoelectric Beams Plates, and Shell,'' *Applied Mechanics Review*, 52:305–320.

Saravanos, D., Heyliger, P. and Hopkins, A. 1997. ''Layer-wise Mechanics and Finite Element for The Dynamic Analysis of Piezoelectric Composite Plates,'' *International Journal of Solids and Structures*, 34:359–378.

Sheikh, A.H., Topdar, P. and Halder, S. 2001. ''An Appropriate Fe Model for Through-thickness Variation of Displacement and Potential in Thin Moderately Thick Smart Laminates,'' *Composite Structures*, 51:401–409.

Shu, X. 2005. ''Free-vibration of Laminated Piezoelectric Composite Plates Based on An Accurate Theory,'' *Composite Structures*, 67:375–382.

Thornbuegh, R.P. and Chattopadhyay, A. 2002. ''Simultaneous Modeling of Mechanical and Electrical Response of Smart Composite Structures,'' *AIAA Journal*, 40:1603–1610.

Tiersten, H.F. 1969. *Linear Piezoelectric Plate Vibrations*, Plenum Press, New York.

Tiersten, H.F. and Mindlin, R.D. 1962. ''Forced Vibrations of Piezoelectric Crystal Plates,'' *Quarterly Applied Mathematics*, 20:107–119.

Wang, J. and Yang, J. 2000. ''High-order Theories of Piezoelectric Plates and Applications,'' *Applied Mechanics Review*, 53:87–96.

APPENDIX

Explicit forms of RMVT-D_z-σ_n Fundamental Nuclei

The stiffness fundamental nucleus $\boldsymbol{K}^{k\tau sij}$ related to the RMVT-D_z-σ_n application is listed below. Constitutive information are included too. In the following, the layer-superscript k is always implied to simplify equations.

The stiffness fundamental nucleus is:

$$K^{\tau sij} = \begin{bmatrix} K_{11} & K_{12} & K_{13} & K_{14} & K_{15} & K_{16} & K_{17} & K_{18} \\ K_{21} & K_{22} & K_{23} & K_{24} & K_{25} & K_{26} & K_{27} & K_{28} \\ K_{31} & K_{32} & K_{33} & K_{34} & K_{35} & K_{36} & K_{37} & K_{38} \\ K_{41} & K_{42} & K_{43} & K_{44} & K_{45} & K_{46} & K_{47} & K_{48} \\ K_{51} & K_{52} & K_{53} & K_{54} & K_{55} & K_{56} & K_{57} & K_{58} \\ K_{61} & K_{62} & K_{63} & K_{64} & K_{65} & K_{66} & K_{67} & K_{68} \\ K_{71} & K_{72} & K_{73} & K_{74} & K_{75} & K_{76} & K_{77} & K_{78} \\ K_{81} & K_{82} & K_{83} & K_{84} & K_{85} & K_{86} & K_{87} & K_{88} \end{bmatrix}. \tag{A.31}$$

Its elements are:

$$\begin{aligned} K_{11} = & \ll F_s F_\tau \gg_z \widetilde{\boldsymbol{H}}_{\text{aa11}} \lhd N_{i,x} N_{j,x} \rhd_\Omega \\ & + \ll F_s F_\tau \gg_z \widetilde{\boldsymbol{H}}_{\text{aa31}} \lhd N_{i,y} N_{j,x} \rhd_\Omega \\ & + \ll F_s F_\tau \gg_z \widetilde{\boldsymbol{H}}_{\text{aa13}} \lhd N_{i,x} N_{j,y} \rhd_\Omega \\ & + \ll F_s F_\tau \gg_z \widetilde{\boldsymbol{H}}_{\text{aa33}} \lhd N_{i,y} N_{j,y} \rhd_\Omega \end{aligned}$$

$$\begin{aligned} K_{21} = & \ll F_s F_\tau \gg_z \widetilde{\boldsymbol{H}}_{\text{aa31}} \lhd N_{i,x} N_{j,x} \rhd_\Omega \\ & + \ll F_s F_\tau \gg_z \widetilde{\boldsymbol{H}}_{\text{aa21}} \lhd N_{i,y} N_{j,x} \rhd_\Omega \\ & + \ll F_s F_\tau \gg_z \widetilde{\boldsymbol{H}}_{\text{aa33}} \lhd N_{i,x} N_{j,y} \rhd_\Omega \\ & + \ll F_s F_\tau \gg_z \widetilde{\boldsymbol{H}}_{\text{aa23}} \lhd N_{i,y} N_{j,y} \rhd_\Omega \end{aligned}$$

$$K_{31} = 0$$

$$K_{41} = 0$$

$$\begin{aligned} K_{51} = & - \ll F_s F_\tau \gg_z \lhd N_i N_{j,x} \rhd_\Omega \widetilde{\boldsymbol{H}}_{\text{ba11}} \\ & - \ll F_s F_\tau \gg_z \lhd N_i N_{j,y} \rhd_\Omega \widetilde{\boldsymbol{H}}_{\text{ba13}} \end{aligned}$$

$$K_{61} = \ll F_\tau F_{s,z} \gg_z \lhd N_i N_j \rhd_\Omega$$

$$K_{71} = 0$$

$$\begin{aligned} K_{81} = & \ll F_s F_\tau \gg_z \lhd N_i N_{j,x} \rhd_\Omega \widetilde{\boldsymbol{H}}_{\text{ba41}} \\ & + \ll F_s F_\tau \gg_z \lhd N_i N_{j,y} \rhd_\Omega \widetilde{\boldsymbol{H}}_{\text{ba43}} \end{aligned}$$

$$\begin{aligned} K_{12} = & \ll F_s F_\tau \gg_z \widetilde{\boldsymbol{H}}_{\text{aa13}} \lhd N_{i,x} N_{j,x} \rhd_\Omega \\ & + \ll F_s F_\tau \gg_z \widetilde{\boldsymbol{H}}_{\text{aa33}} \lhd N_{i,y} N_{j,x} \rhd_\Omega \\ & + \ll F_s F_\tau \gg_z \widetilde{\boldsymbol{H}}_{\text{aa12}} \lhd N_{i,x} N_{j,y} \rhd_\Omega \\ & + \ll F_s F_\tau \gg_z \widetilde{\boldsymbol{H}}_{\text{aa32}} \lhd N_{i,y} N_{j,y} \rhd_\Omega \end{aligned}$$

$$\begin{aligned} K_{22} = & \ll F_s F_\tau \gg_z \widetilde{\boldsymbol{H}}_{\text{aa33}} \lhd N_{i,x} N_{j,x} \rhd_\Omega \\ & + \ll F_s F_\tau \gg_z \widetilde{\boldsymbol{H}}_{\text{aa23}} \lhd N_{i,y} N_{j,x} \rhd_\Omega \\ & + \ll F_s F_\tau \gg_z \widetilde{\boldsymbol{H}}_{\text{aa32}} \lhd N_{i,x} N_{j,y} \rhd_\Omega \\ & + \ll F_s F_\tau \gg_z \widetilde{\boldsymbol{H}}_{\text{aa22}} \lhd N_{i,y} N_{j,y} \rhd_\Omega \end{aligned}$$

$$K_{32} = 0$$

$$K_{42} = 0$$

$$\begin{aligned} K_{52} = & - \ll F_s F_\tau \gg_z \lhd N_i N_{j,x} \rhd_\Omega \widetilde{\boldsymbol{H}}_{\text{ba13}} \\ & - \ll F_s F_\tau \gg_z \lhd N_i N_{j,y} \rhd_\Omega \widetilde{\boldsymbol{H}}_{\text{ba12}} \end{aligned}$$

$$K_{62} = 0$$

$$K_{72} = \ll F_\tau F_{s,z} \gg_z \lhd N_i N_j \rhd_\Omega$$

$$\begin{aligned} K_{82} = & \ll F_s F_\tau \gg_z \lhd N_i N_{j,x} \rhd_\Omega \widetilde{\boldsymbol{H}}_{\text{ba43}} \\ & + \ll F_s F_\tau \gg_z \lhd N_i N_{j,y} \rhd_\Omega \widetilde{\boldsymbol{H}}_{\text{ba42}} \end{aligned}$$

$$K_{13} = 0$$

$$K_{23} = 0$$

$$K_{33} = 0$$

$$K_{43} = 0$$

$$K_{53} = \ll F_{s,z} F_\tau \gg_z \lhd N_i N_j \rhd_\Omega$$

$$K_{63} = \ll F_s F_\tau \gg_z \lhd N_i N_{j,x} \rhd_\Omega$$

$$K_{73} = \ll F_s F_\tau \gg_z \lhd N_i N_{j,y} \rhd_\Omega$$

$$K_{83} = 0$$

$$K_{14} = 0$$

$$K_{24} = 0$$

$$K_{34} = 0$$

$$\begin{aligned} K_{44} = & \ll F_s F_\tau \gg_z \widetilde{\boldsymbol{H}}_{\text{aa44}} \lhd N_{i,x} N_{j,x} \rhd_\Omega \\ & + \ll F_s F_\tau \gg_z \widetilde{\boldsymbol{H}}_{\text{aa54}} \lhd N_{i,y} N_{j,x} \rhd_\Omega \\ & + \ll F_s F_\tau \gg_z \widetilde{\boldsymbol{H}}_{\text{aa45}} \lhd N_{i,x} N_{j,y} \rhd_\Omega \\ & + \ll F_s F_\tau \gg_z \widetilde{\boldsymbol{H}}_{\text{aa55}} \lhd N_{i,y} N_{j,y} \rhd_\Omega \end{aligned}$$

$$K_{54} = 0$$

$$\begin{aligned} K_{64} = & \ll F_s F_\tau \gg_z \lhd N_i N_{j,x} \rhd_\Omega \widetilde{\boldsymbol{H}}_{\text{ba24}} \\ & + \ll F_s F_\tau \gg_z \lhd N_i N_{j,y} \rhd_\Omega \widetilde{\boldsymbol{H}}_{\text{ba25}} \end{aligned}$$

$$K_{74} = \ll F_s F_\tau \gg_z \lhd N_i N_{j,x} \rhd_\Omega \widetilde{\boldsymbol{H}}_{\mathrm{ba}34} + \ll F_s F_\tau \gg_z \lhd N_i N_{j,y} \rhd_\Omega \widetilde{\boldsymbol{H}}_{\mathrm{ba}35}$$

$$K_{84} = \ll F_{s,z} F_\tau \gg_z \lhd N_i N_j \rhd_\Omega$$

$$K_{15} = \ll F_s F_\tau \gg_z \lhd N_j N_{i,x} \rhd_\Omega \widetilde{\boldsymbol{H}}_{\mathrm{ab}11} + \ll F_s F_\tau \gg_z \lhd N_j N_{i,y} \rhd_\Omega \widetilde{\boldsymbol{H}}_{\mathrm{ab}31}$$

$$K_{25} = \ll F_s F_\tau \gg_z \lhd N_j N_{i,x} \rhd_\Omega \widetilde{\boldsymbol{H}}_{\mathrm{ab}31} + \ll F_s F_\tau \gg_z \lhd N_j N_{i,y} \rhd_\Omega \widetilde{\boldsymbol{H}}_{\mathrm{ab}21}$$

$$K_{35} = \ll F_s F_{\tau,z} \gg_z \lhd N_i N_j \rhd_\Omega$$

$$K_{45} = 0$$

$$K_{55} = - \ll F_s F_\tau \gg_z \lhd N_i N_j \rhd_\Omega \widetilde{\boldsymbol{H}}_{\mathrm{bb}11}$$

$$K_{65} = 0$$

$$K_{75} = 0$$

$$K_{85} = \ll F_s F_\tau \gg_z \lhd N_i N_j \rhd_\Omega \widetilde{\boldsymbol{H}}_{\mathrm{bb}41}$$

$$K_{16} = \ll F_s F_{\tau,z} \gg_z \lhd N_i N_j \rhd_\Omega$$

$$K_{26} = 0$$

$$K_{36} = \ll F_s F_\tau \gg_z \lhd N_j N_{i,x} \rhd_\Omega$$

$$K_{46} = - \ll F_s F_\tau \gg_z \lhd N_j N_{i,x} \rhd_\Omega \widetilde{\boldsymbol{H}}_{\mathrm{ab}42} - \ll F_s F_\tau \gg_z \lhd N_j N_{i,y} \rhd_\Omega \widetilde{\boldsymbol{H}}_{\mathrm{ab}52}$$

$$K_{56} = 0$$

$$K_{66} = - \ll F_s F_\tau \gg_z \lhd N_i N_j \rhd_\Omega \widetilde{\boldsymbol{H}}_{\mathrm{bb}22}$$

$$K_{76} = - \ll F_s F_\tau \gg_z \lhd N_i N_j \rhd_\Omega \widetilde{\boldsymbol{H}}_{\mathrm{bb}32}$$

$$K_{86} = 0$$

$$K_{17} = 0$$

$$K_{27} = \ll F_s F_{\tau,z} \gg_z \lhd N_i N_j \rhd_\Omega$$

$$K_{37} = \ll F_s F_\tau \gg_z \lhd N_j N_{i,y} \rhd_\Omega$$

$$K_{47} = - \ll F_s F_\tau \gg_z \lhd N_j N_{i,x} \rhd_\Omega \widetilde{\boldsymbol{H}}_{\mathrm{ab}43} - \ll F_s F_\tau \gg_z \lhd N_j N_{i,y} \rhd_\Omega \widetilde{\boldsymbol{H}}_{\mathrm{ab}53}$$

$$K_{57} = 0$$

$$K_{67} = - \ll F_s F_\tau \gg_z \lhd N_i N_j \rhd_\Omega \widetilde{\boldsymbol{H}}_{\mathrm{bb}23}$$

$$K_{77} = - \ll F_s F_\tau \gg_z \lhd N_i N_j \rhd_\Omega \widetilde{\boldsymbol{H}}_{\mathrm{bb}33}$$

$$K_{87} = 0$$

$$K_{18} = - \ll F_s F_\tau \gg_z \lhd N_j N_{i,x} \rhd_\Omega \widetilde{\boldsymbol{H}}_{\mathrm{ab}14} - \ll F_s F_\tau \gg_z \lhd N_j N_{i,y} \rhd_\Omega \widetilde{\boldsymbol{H}}_{\mathrm{ab}34}$$

$$K_{28} = - \ll F_s F_\tau \gg_z \lhd N_j N_{i,x} \rhd_\Omega \widetilde{\boldsymbol{H}}_{\mathrm{ab}34} - \ll F_s F_\tau \gg_z \lhd N_j N_{i,y} \rhd_\Omega \widetilde{\boldsymbol{H}}_{\mathrm{ab}24}$$

$$K_{38} = 0$$

$$K_{48} = \ll F_s F_{\tau,z} \gg_z \lhd N_i N_j \rhd_\Omega$$

$$K_{58} = \ll F_s F_\tau \gg_z \lhd N_i N_j \rhd_\Omega \widetilde{\boldsymbol{H}}_{\mathrm{bb}14}$$

$$K_{68} = 0$$

$$K_{78} = 0$$

$$K_{88} = - \ll F_s F_\tau \gg_z \lhd N_i N_j \rhd_\Omega \widetilde{\boldsymbol{H}}_{\mathrm{bb}44}$$

Subscripts after comma indicates derivatives,

$$\lhd(\ldots..)\rhd_\Omega = \int_\Omega (\ldots..)\mathrm{d}\Omega \text{ and } \ll(\ldots..)\gg_z = \int_z (\ldots..)\mathrm{d}z.$$

The explicit form of matrices $\widetilde{\boldsymbol{H}}_{aa}$, $\widetilde{\boldsymbol{H}}_{ba}$, $\widetilde{\boldsymbol{H}}_{ab}$ and $\widetilde{\boldsymbol{H}}_{bb}$ is:

$$\widetilde{\boldsymbol{H}}_{aa}(1,1) = C_{11} + \frac{C_{33}e_{31}^2 - C_{13}(2e_{31}e_{33} + C_{13}\varepsilon_{33})}{e_{33}^2 + C_{33}\varepsilon_{33}}$$

$$\widetilde{\boldsymbol{H}}_{aa}(1,2) = \frac{\begin{array}{r} e_{33}(-C_{13}e_{32} + C_{12}e_{33}) + C_{33}(e_{31}e_{32} + C_{12}\varepsilon_{33}) \\ -C_{23}(e_{31}e_{33} + C_{13}\varepsilon_{33}) \end{array}}{e_{33}^2 + C_{33}\varepsilon_{33}}$$

$$\widetilde{\boldsymbol{H}}_{aa}(1,3) = C_{16} + \frac{(C_{33}e_{31} - C_{13}e_{33})e_{36} - C_{36}(e_{31}e_{33} + C_{13}\varepsilon_{33})}{e_{33}^2 + C_{33}\varepsilon_{33}}$$

$$\widetilde{\boldsymbol{H}}_{aa}(1,4) = 0$$

$$\widetilde{\boldsymbol{H}}_{aa}(1,5) = 0$$

$$\widetilde{\boldsymbol{H}}_{aa}(2,1) = \frac{\begin{array}{r} e_{33}(-C_{13}e_{32} + C_{12}e_{33}) + C_{33}(e_{31}e_{32} + C_{12}\varepsilon_{33}) \\ -C_{23}(e_{31}e_{33} + C_{13}\varepsilon_{33}) \end{array}}{e_{33}^2 + C_{33}\varepsilon_{33}}$$

$$\widetilde{\boldsymbol{H}}_{aa}(2,2) = C_{22} + \frac{C_{33}e_{32}^2 - C_{23}(2e_{32}e_{33} + C_{23}\varepsilon_{33})}{e_{33}^2 + C_{33}\varepsilon_{33}}$$

$$\widetilde{\boldsymbol{H}}_{aa}(2,3) = C_{26} + \frac{(C_{33}e_{32} - C_{23}e_{33})e_{36} - C_{36}(e_{32}e_{33} + C_{23}\varepsilon_{33})}{e_{33}^2 + C_{33}\varepsilon_{33}}$$

$$\widetilde{\boldsymbol{H}}_{aa}(2,4) = 0$$

$$\widetilde{\boldsymbol{H}}_{aa}(2,5) = 0$$

$$\widetilde{\boldsymbol{H}}_{aa}(3,1) = C_{16} + \frac{(C_{33}e_{31} - C_{13}e_{33})e_{36} - C_{36}(e_{31}e_{33} + C_{13}\varepsilon_{33})}{e_{33}^2 + C_{33}\varepsilon_{33}}$$

$$\widetilde{\boldsymbol{H}}_{aa}(3,2) = C_{26} + \frac{(C_{33}e_{32} - C_{23}e_{33})e_{36} - C_{36}(e_{32}e_{33} + C_{23}\varepsilon_{33})}{e_{33}^2 + C_{33}\varepsilon_{33}}$$

$$\widetilde{\boldsymbol{H}}_{aa}(3,3) = C_{66} + \frac{-2C_{36}e_{33}e_{36} + C_{33}e_{36}^2 - C_{36}^2\varepsilon_{33}}{e_{33}^2 + C_{33}\varepsilon_{33}}$$

$$\widetilde{\boldsymbol{H}}_{aa}(3,4) = 0$$

$$\widetilde{\boldsymbol{H}}_{aa}(3,5) = 0$$

$$\widetilde{\boldsymbol{H}}_{aa}(4,1) = 0$$

$$\widetilde{\boldsymbol{H}}_{aa}(4,2) = 0$$

$$\widetilde{\boldsymbol{H}}_{aa}(4,3) = 0$$

$$\widetilde{\boldsymbol{H}}_{aa}(4,4) = \frac{C_{55}e_{14}^2 - 2C_{45}e_{14}e_{15} + C_{44}e_{15}^2}{C_{45}^2 - C_{44}C_{55}} - \varepsilon_{11}$$

$$\widetilde{\boldsymbol{H}}_{aa}(4,5) = \frac{C_{55}e_{14}e_{24} + C_{44}e_{15}e_{25} - C_{45}(e_{15}e_{24} + e_{14}e_{25})}{C_{45}^2 - C_{44}C_{55}} - \varepsilon_{12}$$

$$\widetilde{\boldsymbol{H}}_{aa}(5,1) = 0$$

$$\widetilde{\boldsymbol{H}}_{aa}(5,2) = 0$$

$$\widetilde{\boldsymbol{H}}_{aa}(5,3) = 0$$

$$\widetilde{\boldsymbol{H}}_{aa}(5,4) = \frac{C_{55}e_{14}e_{24} + C_{44}e_{15}e_{25} - C_{45}(e_{15}e_{24} + e_{14}e_{25})}{C_{45}^2 - C_{44}C_{55}} - \varepsilon_{12}$$

$$\widetilde{\boldsymbol{H}}_{aa}(5,5) = \frac{C_{55}e_{24}^2 - 2C_{45}e_{24}e_{25} + C_{44}e_{25}^2}{C_{45}^2 - C_{44}C_{55}} - \varepsilon_{22}$$

$$\widetilde{\boldsymbol{H}}_{ab}^T = \begin{bmatrix} \frac{e_{31}e_{33}+C_{13}\varepsilon_{33}}{e_{33}^2+C_{33}\varepsilon_{33}} & 0 & 0 & \frac{C_{33}e_{31}-C_{13}e_{33}}{e_{33}^2+C_{33}\varepsilon_{33}} \\ \frac{e_{32}e_{33}+C_{23}\varepsilon_{33}}{e_{33}^2+C_{33}\varepsilon_{33}} & 0 & 0 & \frac{C_{33}e_{32}-C_{23}e_{33}}{e_{33}^2+C_{33}\varepsilon_{33}} \\ \frac{e_{33}e_{36}+C_{36}\varepsilon_{33}}{e_{33}^2+C_{33}\varepsilon_{33}} & 0 & 0 & \frac{-C_{36}e_{33}+C_{33}e_{36}}{e_{33}^2+C_{33}\varepsilon_{33}} \\ 0 & \frac{-C_{45}e_{14}+C_{44}e_{15}}{C_{45}^2-C_{44}C_{55}} & \frac{C_{55}e_{14}-C_{45}e_{15}}{C_{45}^2-C_{44}C_{55}} & 0 \\ 0 & \frac{-C_{45}e_{24}+C_{44}e_{25}}{C_{45}^2-C_{44}C_{55}} & \frac{C_{55}e_{24}-C_{45}e_{25}}{C_{45}^2-C_{44}C_{55}} & 0 \end{bmatrix};$$

$$\widetilde{\boldsymbol{H}}_{ba} = \begin{bmatrix} -\frac{e_{31}e_{33}+C_{13}\varepsilon_{33}}{e_{33}^2+C_{33}\varepsilon_{33}} & -\frac{e_{32}e_{33}+C_{23}\varepsilon_{33}}{e_{33}^2+C_{33}\varepsilon_{33}} & -\frac{e_{33}e_{36}+C_{36}\varepsilon_{33}}{e_{33}^2+C_{33}\varepsilon_{33}} & 0 & 0 \\ 0 & 0 & 0 & \frac{C_{45}e_{14}-C_{44}e_{15}}{C_{45}^2-C_{44}C_{55}} & \frac{C_{45}e_{24}-C_{44}e_{25}}{C_{45}^2-C_{44}C_{55}} \\ 0 & 0 & 0 & \frac{-C_{55}e_{14}+C_{45}e_{15}}{C_{45}^2-C_{44}C_{55}} & \frac{-C_{55}e_{24}+C_{45}e_{25}}{C_{45}^2-C_{44}C_{55}} \\ \frac{-C_{33}e_{31}+C_{13}e_{33}}{e_{33}^2+C_{33}\varepsilon_{33}} & \frac{-C_{33}e_{32}+C_{23}e_{33}}{e_{33}^2+C_{33}\varepsilon_{33}} & \frac{C_{36}e_{33}-C_{33}e_{36}}{e_{33}^2+C_{33}\varepsilon_{33}} & 0 & 0 \end{bmatrix}.$$

$$\widetilde{\boldsymbol{H}}_{bb} = \begin{bmatrix} \frac{1}{C_{33}+e_{33}^2/\varepsilon_{33}} & 0 & 0 & -\frac{e_{33}}{e_{33}^2+C_{33}\varepsilon_{33}} \\ 0 & \frac{1}{-C_{45}^2/C_{44}+C_{55}} & \frac{C_{45}}{C_{45}^2-C_{44}C_{55}} & 0 \\ 0 & \frac{C_{45}}{C_{45}^2-C_{44}C_{55}} & \frac{1}{C_{44}-C_{45}^2/C_{55}} & 0 \\ -\frac{e_{33}}{e_{33}^2+C_{33}\varepsilon_{33}} & 0 & 0 & -\frac{1}{e_{33}^2/C_{33}+\varepsilon_{33}} \end{bmatrix}.$$